SMC-TR-94-03

AEROSPACE REPORT NO.
TR-93(3940)-9

CDAW-9 Analysis of Magnetospheric Events on 3 May 1986: Event C

1 October 1993

Prepared by

D. N. BAKER, T. I. PULKKINEN, and R. L. McPHERRON
NASA/Goddard Space Flight Center

J. D. CRAVEN
University of Alaska

L. A. FRANK
University of Iowa

R. D. ELPHINSTONE and J. S. MURPHREE
University of Calgary

J. F. FENNELL
Space and Environment Technology Center
Technology Operations
The Aerospace Corporation

R. E. LOPEZ
University of Maryland

T. NAGAI
Meterological Research Institute

and

G. ROSTOKER
University of Alberta

Prepared for

SPACE AND MISSILE SYSTEMS CENTER
AIR FORCE MATERIEL COMMAND
2430 E. El Segundo Boulevard
Los Angeles Air Force Base, CA 90245

Engineering and Technology Group

THE AEROSPACE CORPORATION
Segundo, California

This report was submitted by The Aerospace Corporation, El Segundo, CA 90245-4691, under Contract No. F04701-88-C-0089 with the Space and Missile Systems Center, 2430 E. El Segundo Blvd., Suite 6037, Los Angeles AFB, CA 90245-4687. It was reviewed and approved for The Aerospace Corporation by A. B. Christensen, Principal Director, Space and Environment Technology Center. Major Leslie O. Belsma was the project officer for the Mission-Oriented Investigation and Experimentation (MOIE) program.

This report has been reviewed by the Public Affairs Office (PAS) and is releasable to the National Technical Information Service (NTIS). At NTIS, it will be available to the general public, including foreign nationals.

This technical report has been reviewed and is approved for publication. Publication of this report does not constitute Air Force approval of the report's findings or conclusions. It is published only for the exchange and stimulation of ideas.

Leslie O. Belsma, MAJ, USAF
MOIE Program Manager

WILLIAM KYLE SNEDDON, Capt, USAF
Deputy Chief
Industrial and International Division

REPORT DOCUMENTATION PAGE

Form Approved
OMB No. 0704-0188

1. AGENCY USE ONLY (*Leave blank*)	2. REPORT DATE	3. REPORT TYPE AND DATES COVERED
	1 October 1993	

4. TITLE AND SUBTITLE

CDAW-9 Analysis of Magnetospheric Events on 3 May 1986: Event C

5. FUNDING NUMBERS

F04701-88-C-0089

6. AUTHOR(S) Baker, D.N.; Pulkkinen, T. I.; McPherron, R. L..; Craven, J. D.; Frank, L. A.; Elphinstone, R. D.; Murphree, J. S.; Fennell, J. F.; Lopez, R. E.; Nagai, T.; and Rostoker, G.

7. PERFORMING ORGANIZATION NAME(S) AND ADDRESS(ES)

The Aerospace Corporation
Technology Operations
El Segundo, CA 90245-4691

8. PERFORMING ORGANIZATION REPORT NUMBER

TR-93(3940)-9

9. SPONSORING/MONITORING AGENCY NAME(S) AND ADDRESS(ES)

Space and Missile Systems Center
Air Force Materiel Command
2430 E. El Segundo Blvd.
Los Angeles Air Force Base, CA 90245

10. SPONSORING/MONITORING AGENCY REPORT NUMBER

SMC-TR-94-03

11. SUPPLEMENTARY NOTES

12a. DISTRIBUTION/AVAILABILITY STATEMENT

Approved for public release; distribution unlimited

12b. DISTRIBUTION CODE

13. ABSTRACT (*Maximum 200 words*)

The ninth Coordinated Data Analysis Workshop (CDAW-9) focussed upon several intervals within the PROMIS period (March-June 1986). Event interval C comprised the period 0000-1200 UT on 3 May1986 which was a highly disturbed time near the end of a geomagnetic storm interval. A very large substorm early in the period commenced at 0111 UT and had a peak AE index value of ~1500 nT. Subsequent activity was lower, but at least three other substorms occurred at 2-3 hour intervals. The substorms on 3 May were well observed by a variety of satellites, including ISEE-1, -2, and IMP-8 in the magnetotail plus SCATHA, GOES, GMS, and LANL spacecraft at or near geostationary orbit. A particularly important feature of the 0111 UT substorm was the simultaneous imaging of the southern auroral oval by DE-1 and of the northern oval by Viking. The excellent constellation of spacecraft near local midnight in the radial range 5-9 R_E made it possible to study the strong cross-tail current development during the substorm growth phase and the current disruption and current wedge development during the expansion phase. We use a time-evolving magnetic field model to map observed auroral features out into the magnetospheric equatorial plane. There was both a dominant eastward and a weaker westward progression of activity following the expansion phase. A clear latitudinal separation of the initial region of auroral brightening and the region of intense westward electrojet current was identified. The combined ground, near-tail, and imaging data for this event provided an unprecedented opportunity to investigate tail current development, field line mapping, and substorm onset mechanisms. We find evidence for strong current diversion within the near-tail plasma sheet during the late growth phase and strong current disruption and field-aligned current formation from deeper in the tail at substorm onset. We conclude that these results are consistent with a model of magnetic neutral line formation in the late growth phase which causes plasma sheet current diversion before the substorm onset. The expansion phase onset occurs considerably later due to reconnection of lobelike magnetic field lines and roughly concurrent cross-tail disruption in the inner plasma sheet region.

14. SUBJECT TERMS		15. NUMBER OF PAGES
Current disruption	Magnetotail currents	58
Geomagnetic storm	Substorm	16. PRICE CODE

17. SECURITY CLASSIFICATION OF REPORT	18. SECURITY CLASSIFICATION OF THIS PAGE	19. SECURITY CLASSIFICATION OF ABSTRACT	20. LIMITATION OF ABSTRACT
Unclassified	Unclassified	Unclassified	

Preface

The authors thank the staff of the National Space Science Data Center for the excellent support provided to the CDAW-9 effort. They also thank R. H. Manka for his organizational efforts. One author (TIP) was a guest at GSFC under the aegis of the U.S./Finnish Bilateral program, while another author (RLM) was a National Research Council Senior Resident Research Associate. All work at GSFC was sponsored by NASA. Work at the University of Iowa was supported by NASA grant NAG5-483. Initial participation by JDC occurred while at the University of Iowa. Research at the University of Alaska was supported by NASA grants NAGW-2735 and NAG5-1915.

Contents

Figures

Figures (continued)

Abstract

The ninth Coordinated Data Analysis Workshop (CDAW-9) focussed upon several intervals within the PROMIS period (March - June 1986). Event interval C comprised the period 0000-1200 UT on 3 May 1986 which was a highly disturbed time near the end of a geomagnetic storm interval. A very large substorm early in the period commenced at 0111 UT and had a peak AE index value of ~ 1500 nT. Subsequent activity was lower, but at least three other substorms occurred at 2-3 hour intervals. The substorms on 3 May were well-observed by a variety of satellites including ISEE-1, -2, and IMP-8 in the magnetotail plus SCATHA, GOES, GMS, and LANL spacecraft at or near geostationary orbit. A particularly important feature of the 0111 UT substorm was the simultaneous imaging of the southern auroral oval by DE-1 and of the northern auroral oval by Viking. The excellent constellation of spacecraft near local midnight in the radial range 5-9 R_E made it possible to study the strong cross-tail current development during the substorm growth phase and the current disruption and current wedge development during the expansion phase. We use a time-evolving magnetic field model to map observed auroral features out into the magnetospheric equatorial plane. There was both a dominant eastward and a weaker westward progression of activity following the expansion phase. A clear latitudinal separation ($\gtrsim 10°$) of the initial region of auroral brightening and the region of intense westward electrojet current was identified. The combined ground, near-tail, and imaging data for this event provided an unprecedented opportunity to investigate tail current development, field line mapping, and substorm onset mechanisms. We find evidence for strong current diversion within the near-tail plasma sheet during the late growth phase and strong current disruption and field-aligned current formation from deeper in the tail at substorm onset. We conclude that these results are consistent with a model of magnetic neutral line formation in the late growth phase which causes plasma sheet current diversion before the substorm onset. The expansion phase onset occurs considerably later due to reconnection of lobe-like magnetic field lines and roughly concurrent cross-tail disruption in the inner plasma sheet region.

Introduction

Key outstanding problems in the study of magnetospheric substorms include the determination of where major instabilities are initiated at substorm onset, what physical processes are involved in the instabilities, and how these instabilities evolve to eventually constitute a global magnetospheric disturbance. New tools to address these issues include multispacecraft observations, global auroral images, and realistic magnetic field mapping capabilities. Coordinated Data Analysis Workshops (CDAWs) have allowed the exploitation of these new tools by making

readily available a wide array of ground-based measurements, high-altitude particle and field data from numerous spacecraft, and auroral imaging sequences from such polar-orbiting satellites as Dynamics Explorer (DE)-1 and Viking.

A period of particularly extensive data collection was the PROMIS (Polar Region Outer Magnetosphere International Study) interval of March-June 1986 (see Hones, 1985). The PROMIS campaign took advantage of the fact that during this interval the Viking spacecraft made frequent observations of the northern polar region while at the same time the DE-1 spacecraft was observing the southern polar region. When it was also recognized that during this period the near-Earth plasma sheet was extensively sampled by such spacecraft as the International Sun-Earth Explorer pair (ISEE-1, -2), a relatively rare possibility existed to study global magnetospheric dynamics. Since these core PROMIS observations could be augmented by various operational spacecraft (e.g., GOES at 6.6 R_E) and by ground-based magnetometers and radars (see Table 1), it was clear that the PROMIS period was an ideal one from which to select several CDAW intervals for detailed analysis.

The PROMIS period designated as the CDAW-9 Event C extended from 0000 to 1200 UT on 3 May 1986. This was a very disturbed period at the end of a geomagnetic storm that had a sudden commencement at ~2010 UT on 1 May 1986. The Event C period had several discrete substorm onsets contained within it (see, for example, Hones et al., 1987). In this report we will focus almost exclusively on the first substorm of 3 May 1986 which had an identified expansion phase onset time of 0111 UT. Because of the very disturbed nature of the magnetosphere at this time, the substorm effects in the magnetotail were exceptionally close to the Earth. This allowed numerous geostationary spacecraft to observe directly the substorm initiation processes. In this report we will demonstrate the localized nature in space and time of the substorm onset and we will map this initiation from ionospheric to magnetospheric altitudes using realistic, temporally-evolving magnetic field models (see Pulkkinen et al., 1991). We will also explore further the cause of the onset of the substorm and we will consider evidence that the ion tearing mode was probably initiated in an extremely thin cross-tail current system at about the time of the substorm expansion phase. These results will be considered in the context of a model of substorms which asserts that a near-Earth magnetic reconnection process is the principal instability causing the substorm onset.

Table 1. Observation Facilities for PROMIS

Region	Promis (March-June 1986)
Solar Wind	IMP 8
Polar Magnetosphere and Imaging	Viking (north) DE 1 (south) DMSP F7
Inner Magnetosphere	6 Geosynchronous Scatha AMPTE-CCE
Outer Magnetosphere	ISEE 1 ISEE 2 AMPTE IRM IMP 8
Distant Tail	———
Ground	EISCAT radar Sondrestrom radar STARE radar Magnetometer arrays CANOPUS

Event Overview

The lower part of Figure 1 shows the 12-station AE index (Davis and Sugiura, 1966) for the entirety of the Event C period (0000-1200 UT). There were obvious isolated substorm intervals identifiable in the record beginning at ~0130 UT, ~0430 UT, ~0530 UT, ~0715 UT, and ~0920 UT. Thus, the geomagnetic activity tended to recur every two to three hours. The peak AE in each successive episode of activity diminished from the peak in the prior episode. The overall background level of AE also decreased throughout this period as the geomagnetic storm decayed and the magnetosphere recovered toward prestorm conditions.

The upper portion of Figure 1 shows a detail of the auroral zone geomagnetic record for 0000 to 0400 UT on 3 May 1986. The AU and AL indices are plotted (where, by definition, AE ≡ AU-AL). If one identifies the largest sudden decrease in AL with the substorm expansion phase onset (e.g., Rostoker et al., 1980), then one would conclude from Fig. 1b that the onset was at ~0130 UT. As we will show here, however other data suggest a considerably earlier onset time. The minimum value of AL, corresponding to the maximum westward electrojet, was ~ -1150 nT and this occurred at ~0140 UT. The lack of detailed correspondence between AL index timing and other measures of substorm onset may be related to the limited number of stations and the station coverage used in the computation of the indices.

Ground signatures of the substorm timing may be compared in this case with concurrent spacecraft observations, including global auroral imaging results. We present here a broad overview of the imaging data, while later in this paper we will present detailed analyses of the images and their mapping into the magnetospheric equatorial plane. It is perhaps worth noting that we have utilized several different geomagnetic coordinate systems in the overview plots since these different systems happen to be the preferred coordinates of the several research groups involved. Thus, DE-1 data are presented in magnetic latitude - magnetic local time (MLT) coordinates. Viking data are presented in closely analogous eccentric dipole (1985) coordinates. The Greenland magnetometer chain data are presented in terms of invariant latitude (INVL), while the Canadian sector data are presented in terms of corrected geomagnetic latitude. The several magnetic coordinate systems may seem confusing, but they all give generally similar representations (adequately similar, at least, for the overview purposes). Later in this paper, as we do detailed comparisons and mappings, we use all positional information from various sources in geographic coordinates and then transform all of these data into one single coordinate system.

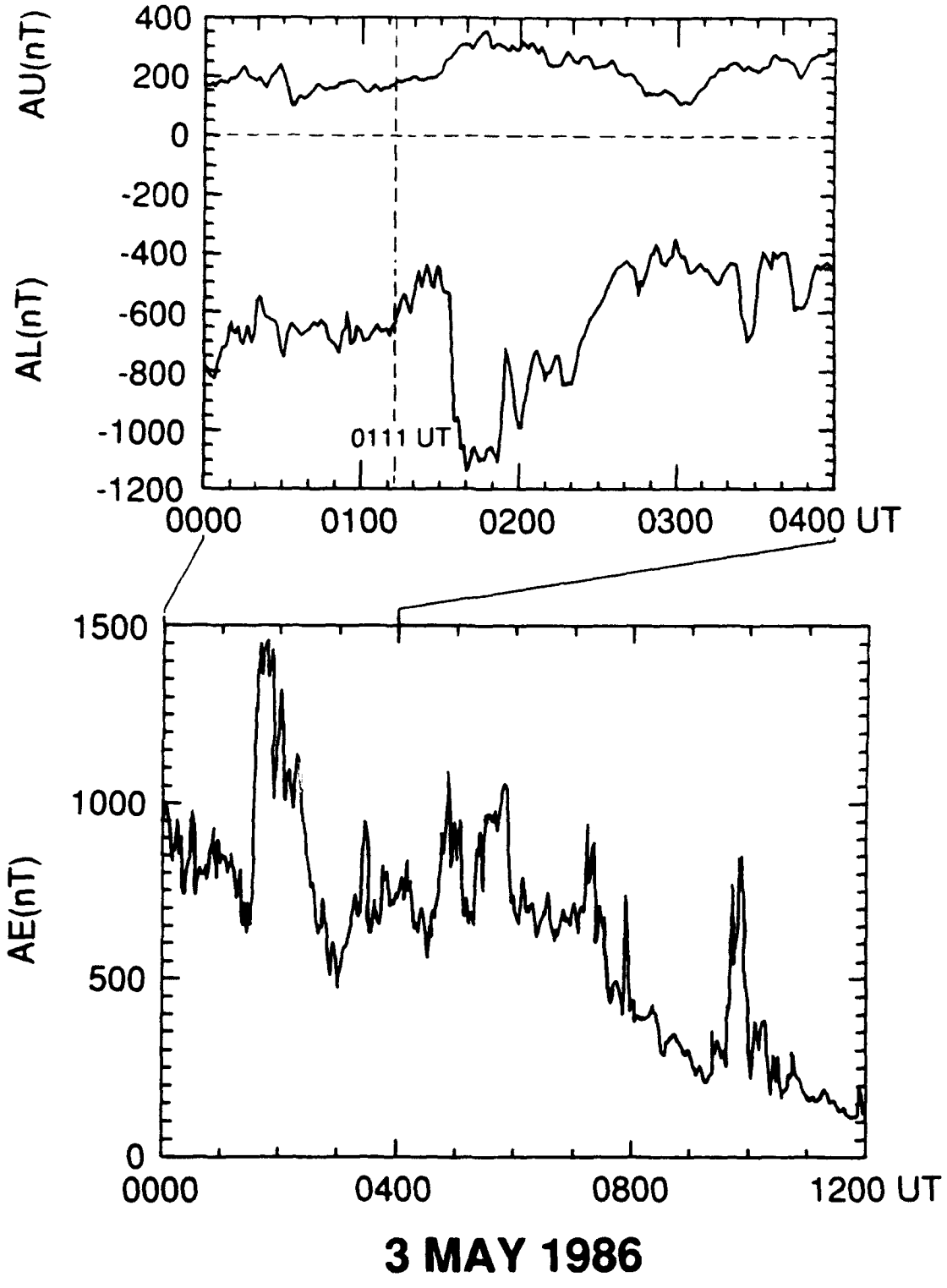

Fig. 1. Auroral electrojet indices (12-station) for a portion of 3 May 1986. The AE index is shown for 0000-1200 UT (Bottom) and the AL and AU indices are shown for 0000-0400 UT (Top).

The DE-1 spacecraft was positioned over the south polar region during the period of the 3 May 1986 event. Complete views of the southern auroral oval were obtained by the imaging experiment (Frank et al., 1981) on DE-1 throughout the period 2352 UT on 2 May to 0347 UT on 3 May. Images were acquired with 8-min resolution at 117-170 nm, for which the principal contributions to the response at auroral latitudes are the emission of OI at 130.4 and 135.6 nm and from the LBH bands of N_2. Contribution due to a weak background of geocoronal Lyman-α emissions is largely eliminated in the presentation used here. A selection of all the available images is used in this analysis. Figure 2 shows a sequence of 9 images beginning at 0000 UT and extending to an image whose acquisition ended at 0137 UT on 3 May. A broad, disturbed auroral oval was seen in the image obtained at 0000 UT. Bright auroral regions were seen extending from ~ 1900 MLT to local midnight. In the postmidnight sector, the auroral oval extended from ~ 60° latitude to ~ 78° latitude. These same general features were seen in the image taken at 0016 UT, but the identifiable auroral oval tended to reduce in latitudinal width compared to the earlier time.

Further quieting of the auroral oval occurred during the period 0032 to 0105 UT. The bright auroras in the premidnight sector lessened in latitudinal and longitudinal width, and the entire oval became substantially narrower in latitudinal extent with time. By 0105 UT, the detectable oval extended from ~ 58° latitude to ~ 66° latitude. Thus, during this general period (0000-0105 UT) there was some equatorward motion of the auroral oval, and the polar cap size increased substantially. In the 0113 UT image, the auroras brightened markedly in the premidnight sector demonstrating a clear substorm onset at about that time. The auroras remained bright, and there were expansions of activity both eastward and westward until at least 0129 UT.

The Viking spacecraft was near apogee over the northern polar region early on 3 May 1986. The imaging experiment (Anger et al., 1987) onboard the spacecraft returned 1-sec snapshot images of the auroral oval at 40-second resolution from 0040:58 UT until 0126:35 UT. A sampling of the available images during this time is shown in Figure 3. At 0048:02 UT, the northern auroral oval was relatively broad, extending from ~ 56° to ~ 68° magnetic latitude in the premidnight sector. There was a distinct equatorward arc system at ~ 60° latitude, but clear auroral luminosity was evident far poleward of this arc. This is a typical configuration observed during active intervals and the recovery phase of a previous substorm (Elphinstone and Hearn, 1992). This "double oval" configuration allows important inferences to be made about the location of the optical substorm onset.

By 0053:44 UT, the Viking imager was able to observe the entire nightside auroral oval. The third image included in Figure 3 (0059:05 UT) reveals the equatorward motion of the most

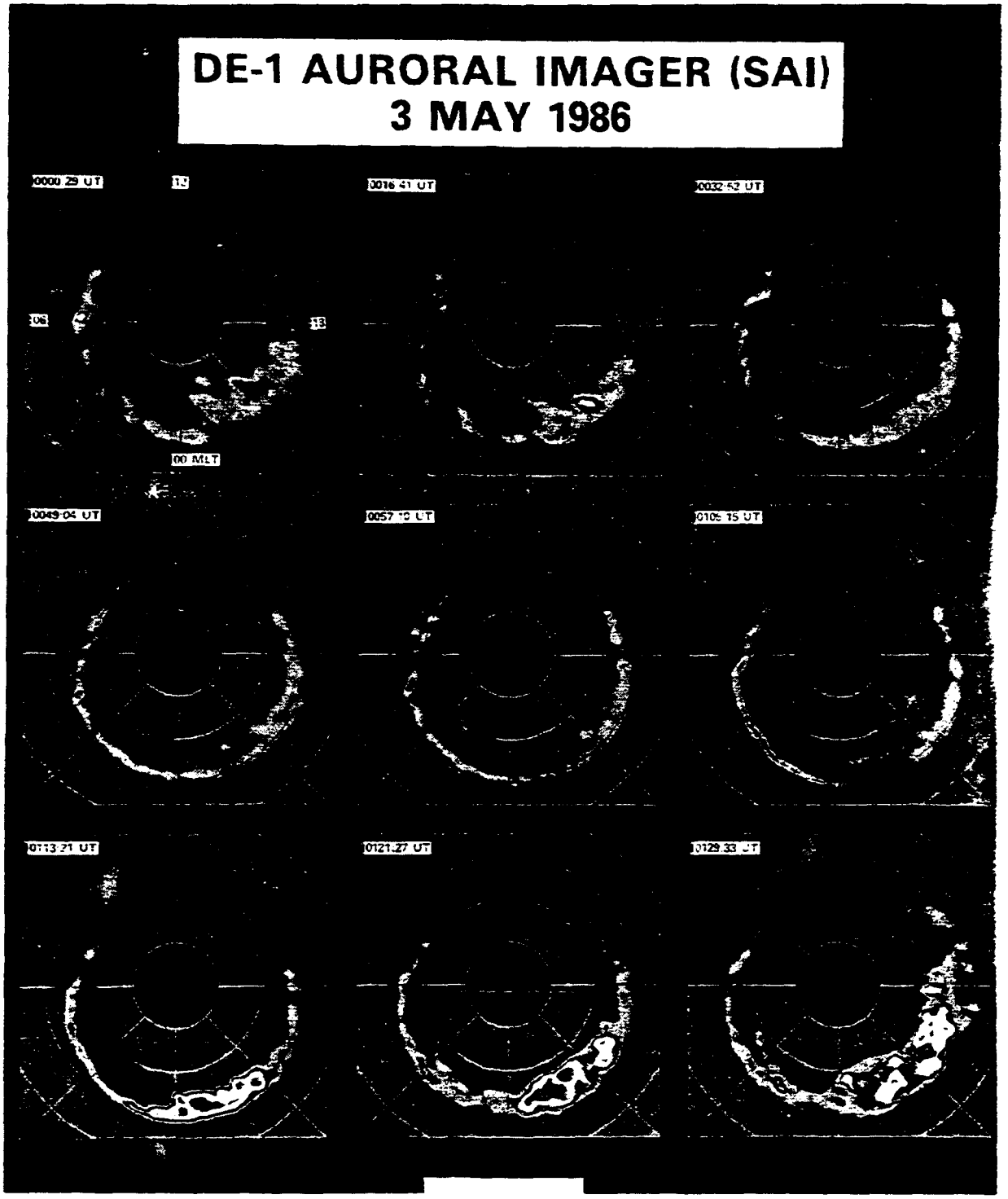

Fig. 2. A sequence of southern auroral images taken by the DE-1 imager with starting accumulation times from 0000-0129 UT on 3 May 1986. Images are shown in magnetic latitude-magnetic local time coordinates. Note that local dawn is toward the left in each image, while local dusk is toward the right (since this is southern hemisphere data). Images are acquired over 8-min intervals.

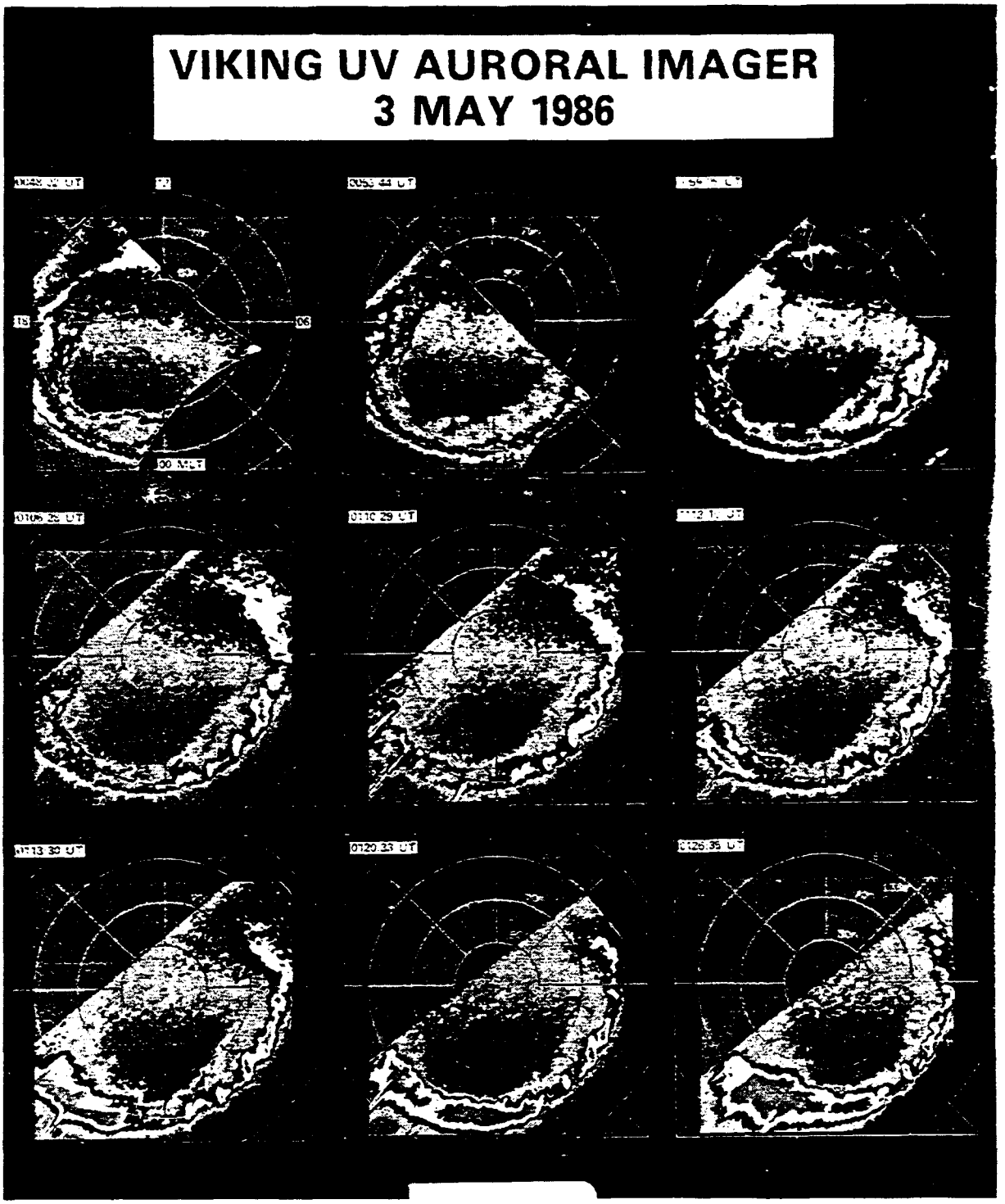

Fig. 3. A sampling of northern auroral images taken by the Viking imager during the period 0040-0126 UT on 3 May 1986. The format is similar to Fig. 2 except that the coordinate system used is eccentric dipole (1985) and dawn and dusk have been reversed for northern hemisphere projection. Images are 1-s snapshots with a basic time resolution for each camera of 40-s.

poleward of the two ovals and suggests development of bright regions on this arc system at ~ 2000 MLT (eccentric dipole 1985 coordinates). Images at 0106:28 UT and 0110:29 UT continued to show a relatively quiet, broad auroral distribution in the premidnight sector. The image acquired at 0112:10 UT shows major brightening of the equatorward arc system near 60° and at ~ 2100 MLT, about two hours west of the mean location for auroral substorm onset as determined with DE-1 (Craven and Frank, 1991). The auroras brightened and expanded away from this location in the subsequent images (0113:30, 0120:33, and 0126:35 UT).

Further definition of the substorm characteristics is possible using individual ground magnetograms as shown in Figure 4. Fig. 4a shows the H-component records for the period 0000-0400 UT on 3 May from the Greenland array (E. Friis-Christensen, private communication). Data from the western coast of Greenland ranging from Thule (THL at 85.8° invariant latitude) down to Narssarsuaq (NAQ at 67.1° INVL) all clearly support the identification of an isolated substorm with maximum development shortly before 0200 UT. In the data records from the auroral latitude stations of Godthab (GHB), Frederikshab (FHB), and Narssarsuaq, the substorm appears as a single episode of activity with the negative bay commencing at ~ 0125 UT. The higher latitude stations such as Sondre Stromfjord (STF, 73.7° INVL) show what appears to be a first onset at ~ 0140 UT and a second intensification near ~ 0200 UT. We would, however, interpret this later feature as being related to the substorm recovery phase and its associated high-latitude current systems.

Ground-based magnetometer data from the Canadian and Alaskan sector are presented in Fig. 4b. This shows the X-component records for the selected stations for the period 0000 - 0400 UT. In some contrast to the Greenland data, the eastern Canadian data (especially Fort Churchill and Poste de la Baleine) reveal gradual negative bay development much earlier beginning at ~ 0110 UT. Fig 4c shows the X, Y, and Z components of the magnetic field for Poste de la Baleine (66.2° CML [corrected geomagnetic latitude]) and Ottawa (56° CML) for the period 0000 - 0400 UT. These two stations are in the same magnetic meridian and were at ~ 2100 MLT at 0100 UT on 3 May. They were evidently the closest stations to the substorm onset sector. The much larger X and Z components of the perturbations seen at PDB compared to Ottawa show that electrojet currents were flowing much closer to magnetic latitude of ~ 66° than 56°. Note that the magnetic disturbances at PDB commenced right at 0111 UT, in excellent agreement with the Viking auroral brightening time. Thus, the imaging data show brightened aurora first at $\leq 60^{\circ}$ magnetic latitude, whereas the magnetometer data suggest that the most intense electrojet currents are located toward the poleward edge of the visible auroral distribution.

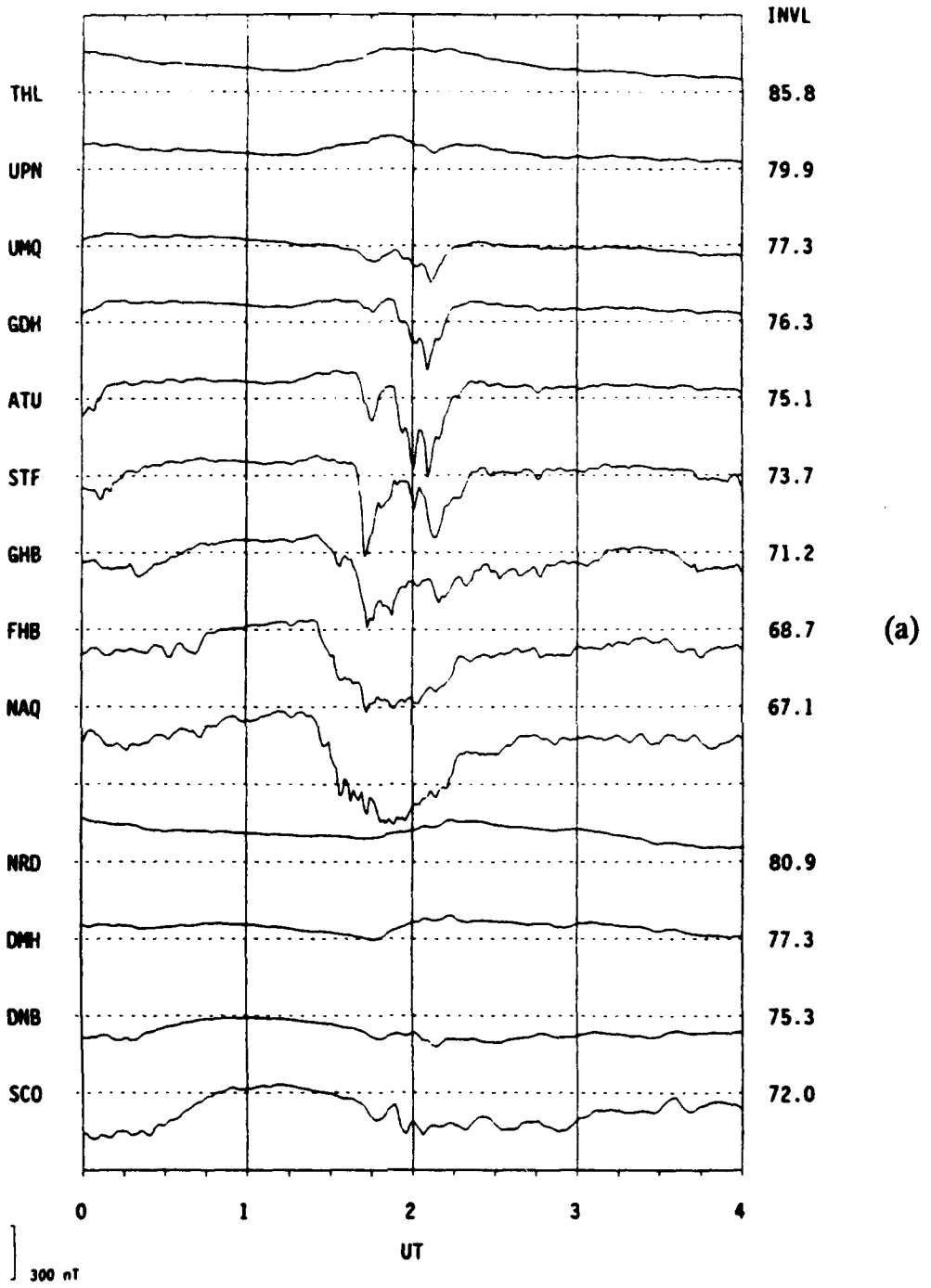

(a)

Fig. 4. (a) Greenland magnetometer chain data (H-component) for 0000-0400 UT on 3 May 1986. (b) Selected Canadian-sector magnetometer data (X-component). (c) X-, Y-, and Z-component magnetometer data from Ottawa (OTT) and Poste de la Baleine (PDB).

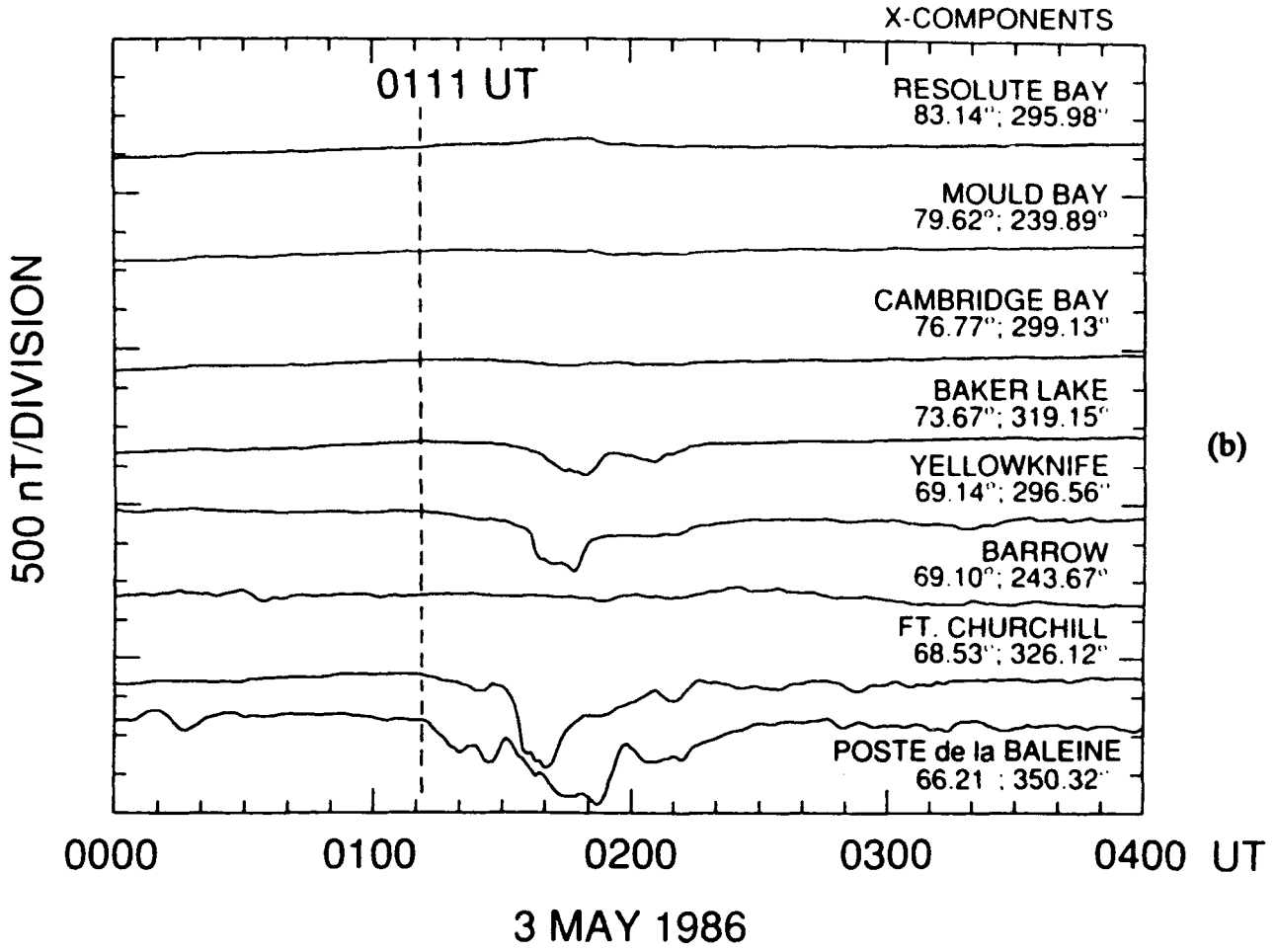

Fig. 4. (a) Greenland magnetometer chain data (H-component) for 0000-0400 UT on 3 May 1986. (b) Selected Canadian-sector magnetometer data (X-component). (c) X-, Y-, and Z-component magnetometer data from Ottawa (OTT) and Poste de la Baleine (PDB).

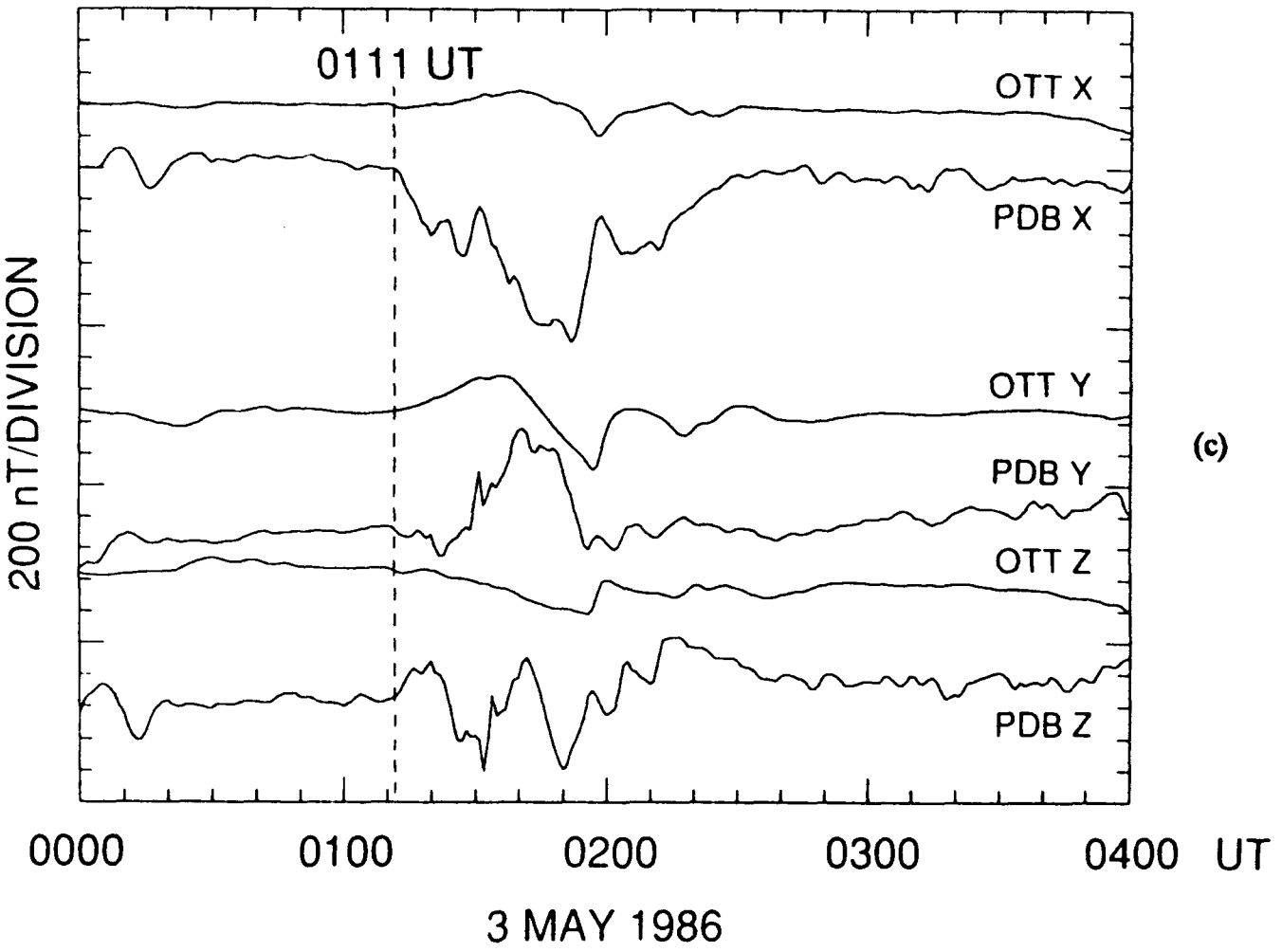

Fig. 4. (a) Greenland magnetometer chain data (H-component) for 0000-0400 UT on 3 May 1986. (b) Selected Canadian-sector magnetometer data (X-component). (c) X-, Y-, and Z-component magnetometer data from Ottawa (OTT) and Poste de la Baleine (PDB).

Based on the auroral electrojet information, we conclude that the early portion of 3 May 1986 was a quite disturbed period. Substorm activity reached its maximum level at ~0140 UT, based upon the time of peak AE value. Concurrent imaging data from DE-1 and Viking in the southern and northern hemispheres, respectively, show that intense auroral brightening occurred at ~ 0111 UT: This is taken as the substorm expansion phase onset time. The low-altitude observations show that immediately after the substorm onset the activity was spread over a region > 10° in latitude, suggesting a near-simultaneous process taking place in large regions of the ionosphere and/or in the magnetospheric regions to which the active regions maps.

Spacecraft Observations

In addition to the imaging data described above, there were a number of other satellite data sets on 3 May 1986 available for analysis. Figure 5 provides the locations of the several spacecraft, from high- to low-altitude, that have been examined in this study. At highest altitude, the IMP-8 spacecraft measured energetic particles and magnetic fields in the mid-magnetotail region throughout the event. Fig. 5a shows that it was located toward the dawn side of the tail at (-31, -10, -1) R_E, in Geocentric Solar Magnetospheric (GSM) coordinates. As will be shown below, IMP-8 was in and out of the distant plasma sheet between 0000 and 0300 UT; it was immersed in the plasma sheet proper at the substorm onset time shortly after 0100 UT.

Figure 5b shows the constellation of spacecraft at, or near, geostationary orbit for the event. Particularly important are the satellites in the midnight and premidnight sector: SCATHA, S/C 1982-019 (S19, hereafter), ISEE-1 (and -2), and GOES-5. As will be demonstrated below, these spacecraft were in the vicinity of the substorm initiation region, and they provided key information concerning the growth phase of the substorm as well.

Finally, Fig. 5c shows the low-altitude configuration of spacecraft with Viking near apogee in the northern polar region and DE-1 near apogee over the southern pole. Also, the Defense Meteorological Support Program (DMSP) F7 spacecraft was operating during this event. From its 840 km altitude circular orbit, DMSP was able to measure auroral particle features just before and just after the substorm expansion phase onset.

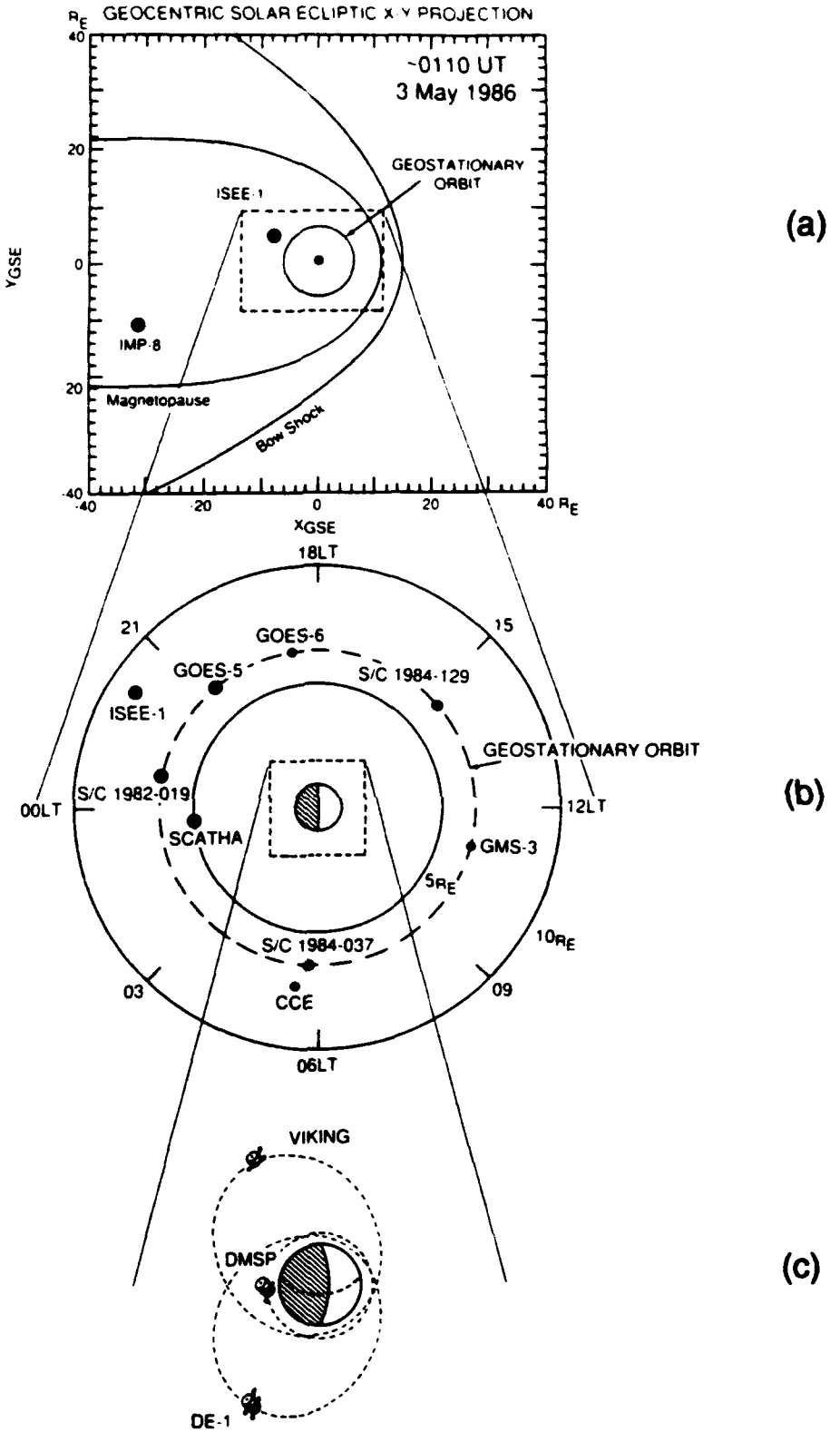

Fig. 5. A summary of satellites (and their locations) available for use in this study. Positions are shown for ~ 0110 UT on 3 May 1986.

Growth Phase Features

From the imaging and ground-based measurements presented in the event overview, we would estimate that at ~ 0100 UT ISEE-1 and GOES-5 were in the general longitude sector of the substorm initiation (i.e., ~ 21 LT). Figure 6 shows magnetic field (Russell et al., 1978) and selected plasma (Frank et al., 1978) data from the ISEE-1 spacecraft. The upper three panels show B_X, B_Y, and B_Z in GSM coordinates for the period 0000 to 0300 UT. During this time, ISEE-1 was outbound at ~ 2200 LT and ~ 9 R_E geocentric distance. A very evident feature of the magnetic measurements is the systematic and progressive "taillike" stretching of the field (see also Pulkkinen et al., 1991). From essentially the beginning of the day until 0111 UT, B_Z substantially diminished and $|B_X|$ generally increased. This is a classic signature of the substorm growth phase (McPherron, 1970). During this same general interval, the plasma ion temperature shown in Fig. 6 decreased progressively, another feature often associated with substorm growth phases (Fairfield et al., 1981).

Other spacecraft in the premidnight sector clearly support the identification of a substorm growth phase between 0000 and ~ 0110 UT. Figure 7 shows GOES-5 magnetic field data for the period 0000 - 0300 UT on 3 May. The spacecraft was near 2000 LT early in this interval, and it observed a progressive and substantial stretching of the field (B_Z decreased and $|B_X|$ increased) very similar to that seen by ISEE-1. Further evidence of the growth phase development is provided by other geostationary orbit spacecraft such as S19 near ~ 2300 LT. As shown in Figure 8, the ~ 30 keV to ~ 200 keV electrons measured by S19 showed a systematic decrease in flux from 0000 UT until at least 0045 UT. The higher energy electron fluxes showed a complete "dropout" and were then at background until the substorm onset time. The S19 data also revealed a progressive development of a "cigarlike" anisotropy of the energetic electrons (data not shown here) during this same interval. These flux and anisotropy features at geosynchronous orbit are traditional, highly repetitive features of the substorm growth phase (Baker et al., 1978).

Finally, the SCATHA spacecraft (Fennell, 1982) also made measurements slightly inside geostationary orbit (r ~ 5 R_E) during this interval. The SCATHA magnetic field and selected energetic particle data for the period 0000 to 0300 UT are shown in Figure 9. Generally speaking, the SCATHA data exhibit the same features seen at ISEE, GOES, and S19: There was a progressive taillike stretching of the magnetic field (0000 ~ 0110 UT) and a progressive decrease in the energetic particle flux. Thus, the 70-min period prior to ~0110 UT would be taken as the energy storage interval (e.g., Baker et al., 1984) in which tail energy was loaded prior to the unloading phase commencing at ~ 0111 UT.

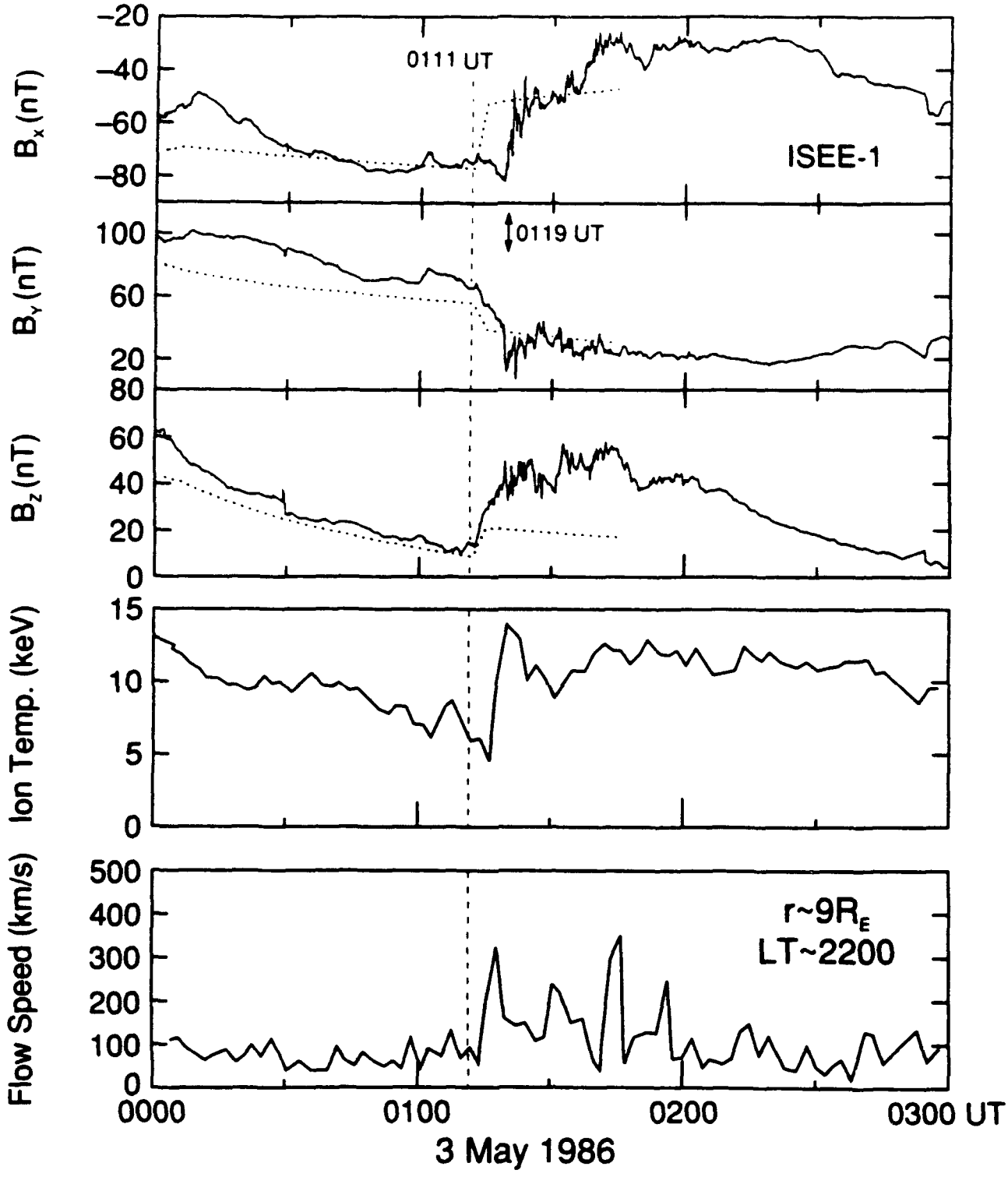

Fig. 6. Selected magnetic field (upper 3 panels) and plasma (lower panels) data from ISEE-1 for the period 0000 - 0300 UT on 3 May 1986. The dotted lines accompanying the magnetic field data show model fits as described in the text.

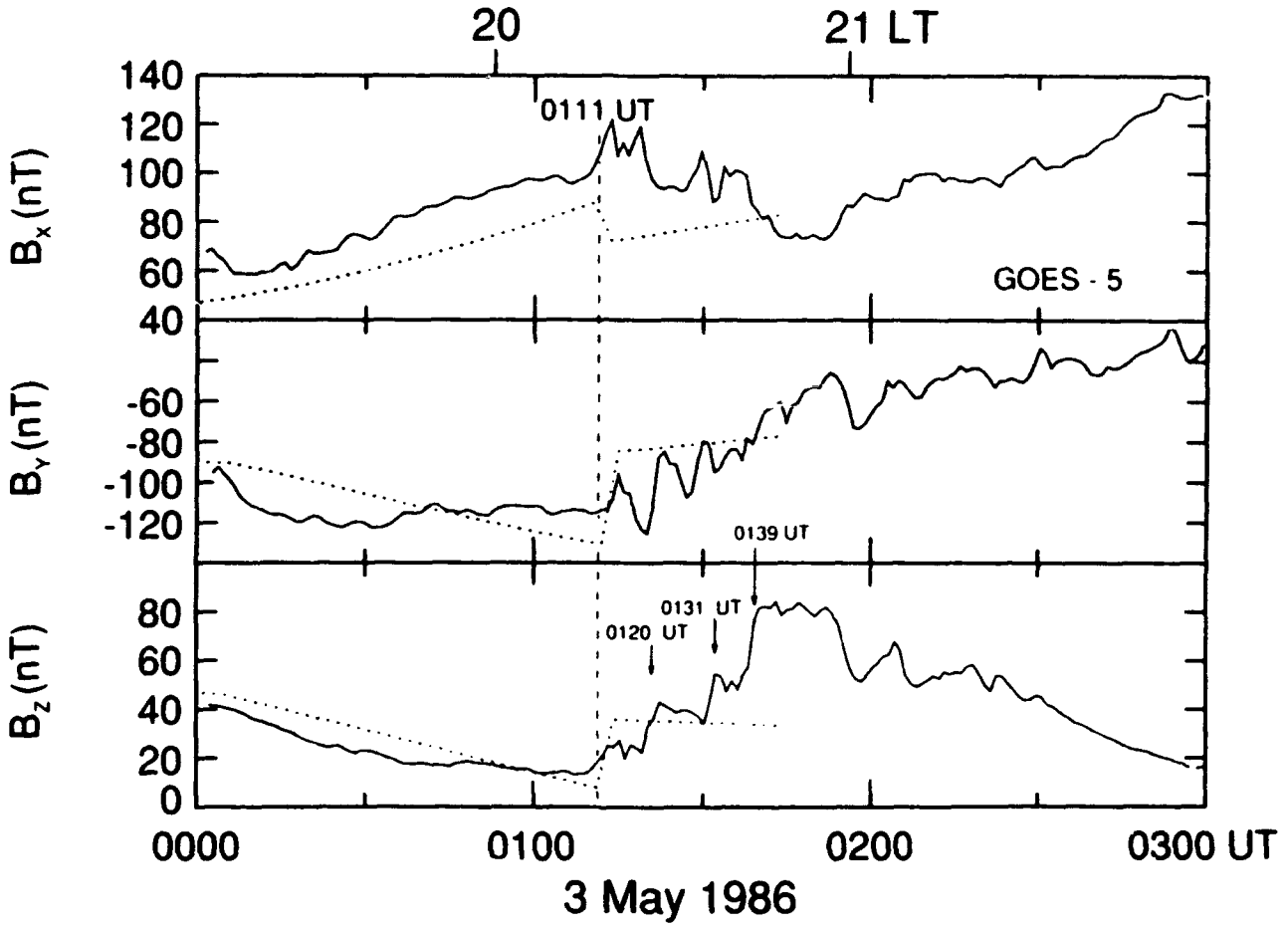

Fig. 7. Magnetic field data from GOES-5 at geostationary orbit for 0000 -0300 UT on 3 May 1986. The dotted lines in the magnetic field panels show the model fits derived for the growth phase of the 0111 UT substorm as described in the text.

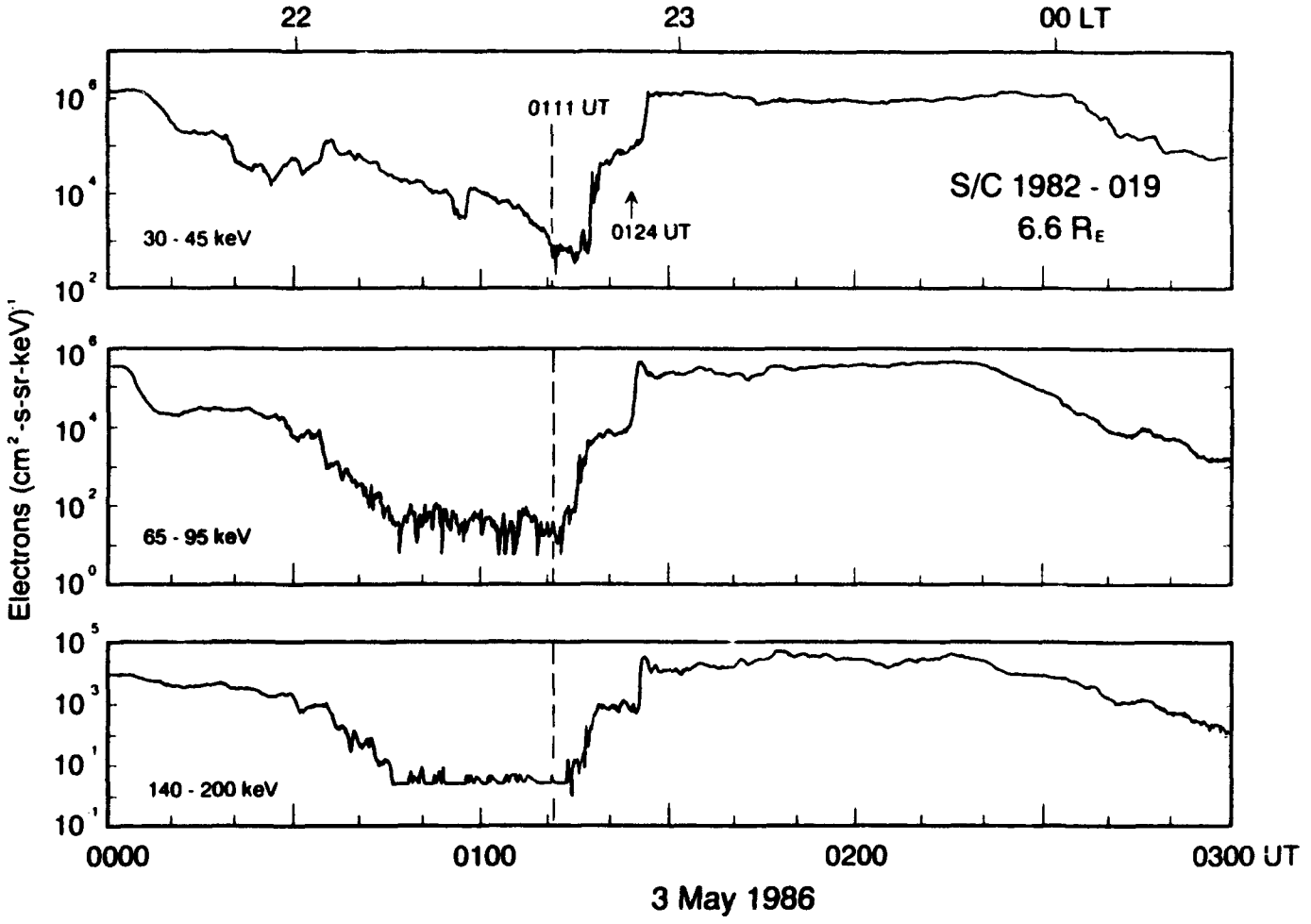

Fig. 8. Selected energetic electron data for S/C 1986-019 (S19) for the period 0000-0300 UT on 3 May 1986.

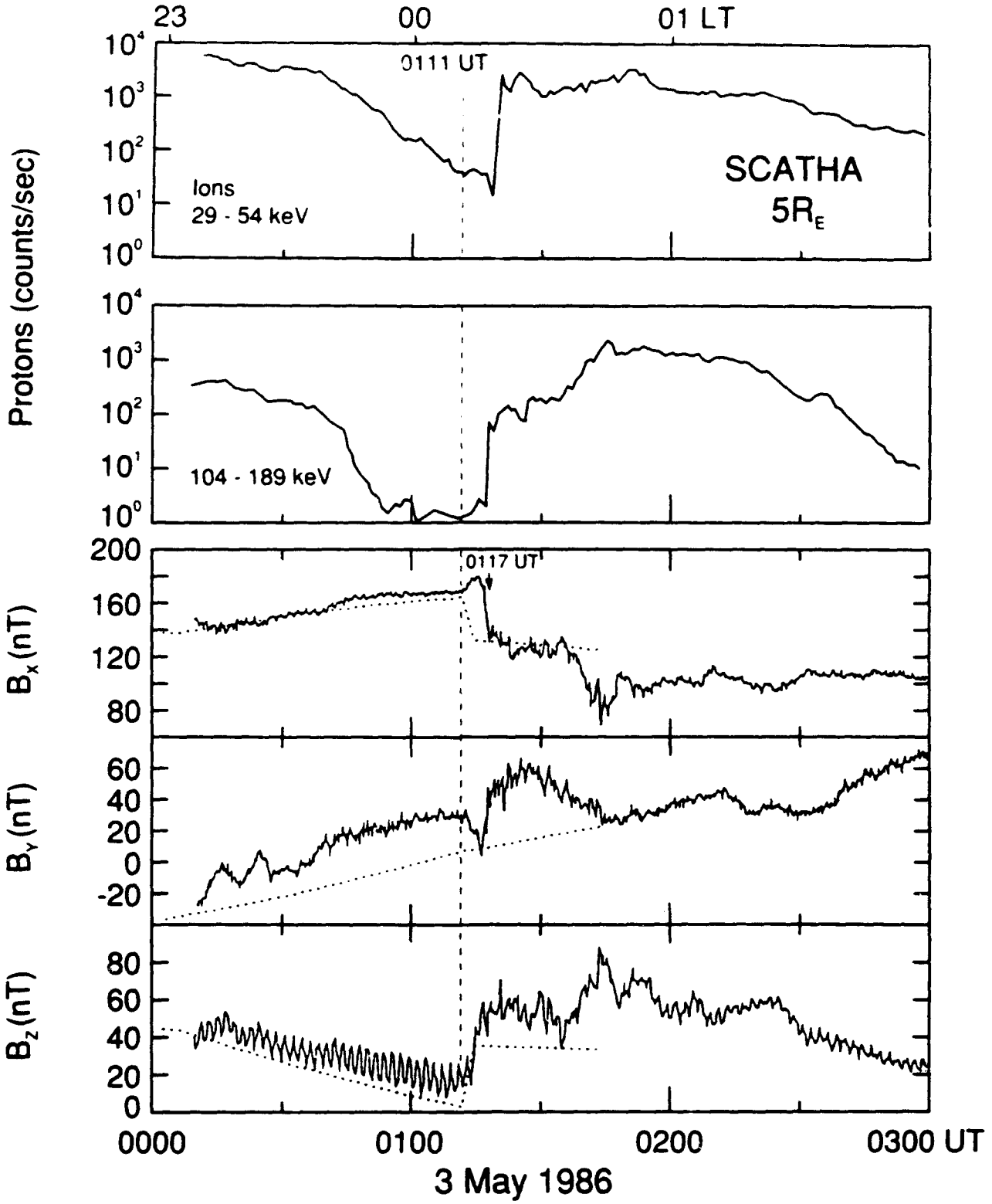

Fig 9. Energetic ion (top panels) and magnetic field (lower panels) data from the SCATHA spacecraft. The dotted curves show model fits to the magnetic field components as described in the text.

Magnetic Modeling of the Growth Phase

The data in Figures 6-9 show relatively strong, but familiar, patterns associated with the substorm growth phase (McPherron, 1970; Baker et al., 1978). The loading of energy into the magnetotail from the solar wind causes a substantial increase of magnetic energy in the tail lobes. This increasing magnetic flux in the lobes is directly associated with an increase in the cross-tail current. The extreme tail-like stretching of the field close to the Earth ($r \sim 6\ R_E$) late in the growth phase requires an intense, thin current sheet in the near-tail equatorial plane (Kaufmann, 1987; Baker and McPherron, 1990). The stretched field and the very thin current sheet just before expansion onset leads to substantial energetic particle dropouts.

In this report we wish to relate auroral and low-altitude current features to measurements made from satellites in the equatorial plane. Many researchers have recently used the empirical magnetic field models of Tsyganenko (1987, 1989) to map from one part of the magnetosphere (or ionosphere) to another (see, for example, Elphinstone et al., 1991; Birn et al., 1991). The Tsyganenko (1989) magnetic field model gives the Earth's magnetic field as a sum of terms representing each of the magnetospheric current systems. The ring current and the tail current are confined to the equatorial plane, while the Chapman-Ferraro term and the cross-tail closure current term represent the currents at the dayside and nightside magnetospheric boundaries, respectively. The model field is given as a function of the magnetic dipole tilt angle between the Sun-Earth line and the dipole equator, and the Kp–index indicating the level of geomagnetic activity. The internal geomagnetic field contribution is derived using the IGRF 1985 coefficients. Modifications to such a magnetic field model have been used to successfully reproduce satellite magnetic field observations during the growth phase (see, for example, Lui, 1978; Sergeev et al., 1990; Pulkkinen et al., 1991).

The growth phase effects for the period 0000-0110 UT on 3 May have been included in the basic Tsyganenko (1989) model by varying the model parameters and by modification of the functional form of the field components (Pulkkinen, 1991; Pulkkinen et al., 1991). The current sheet was locally thinned by modification of the function representing the current sheet thickness for X and Y positions in the model. Pulkkinen et al. (1991) determined the minimum thickness, location of the minimum thickness, and size of the thinned region as free parameters. The enhanced tail magnetic flux was represented by increasing the model tail current intensity by a factor of $(1 + f)$, which produced appropriate enhancement of the field terms. Pulkkinen et al. noted that because the usual (Tsyganenko, 1989) model tail current peaks beyond 10 R_E, its enhancement does not account adequately for stretching of the field in the region between 5 and 10

R_E. In order to further increase the taillike stretching close to the Earth, a new current sheet was added to the model. The functional form of the new current sheet was chosen to be similar to the ring current. The peak intensity, location of the current maximum, and the thickness of the added current sheet was set according to the observed degree of field stretching. Thus, the modifications of the Tsyganenko (1989) model were represented by a group of parameters whose values were set by a least-squares type of comparison with the field observations (see also Pulkkinen et al., 1992).

The modified magnetic field model for the growth phase on 3 May 1986 was constructed by assuming that the field near the beginning of the growth phase (0000 UT) could be represented by the unmodified Tsyganenko model using its highest selectable level of magnetic activity, $Kp \geq 5^-$. Temporal development was then obtained by changing parameters linearly with time to describe the enhancement of the currents until the substorm onset at ~ 0111 UT. The minimum thickness of the current sheet, the intensification of the tail and ring currents, and the peak intensity of the newly-added current sheet near Earth were varied during that period. All remaining seven parameters out of the total of 11 parameters in the model maintained the constant values used at the beginning of the growth phase. As noted by Pulkkinen et al. (1991), the parameters giving the current intensity resulting from the various terms affect principally the X-component field, while the current sheet minimum thickness and location, as well as the location of the new current sheet, have largest effect on the Z-component in the model. Since the time-varying currents all are azimuthal, the time-dependent modifications do not produce significant effects on the Y-component of the field in the midnight sector.

To obtain the optimal correspondence with the observations from all spacecraft in this case, the current sheet was thinned until it reached a minimum thickness which was only 10% of the original value (which, at X ~ -10 R_E, was about 4 R_E). The tail flux was enhanced by a factor of 1.2 (i.e., $f = 0.2$). The additional thin current sheet added to the model had a peak intensity which was 55% of the ring current intensity and a current maximum located at 4.7 R_E. The thickness of this current sheet was 10% of the thickness of the ring current at that location.

The dashed lines in Figures 6, 7 and 9 show the model fits to the measured near-tail magnetic field components between 0000 UT and 0112 UT. At 0112 UT the model was allowed to transition back (over a 2-min interval) to the Tsyganenko (1989) representation. The dashed line in each case between ~ 0115 UT and 0140 UT simply shows the unmodified Tsyganenko model representation for the location of the respective spacecraft.

Fig. 6 shows that the ISEE-1 B_x and B_z model fits are generally quite good throughout the growth phase. The discontinuity in the ISEE field components, most notably the B_z component, at ~ 0028 UT is due to a sensor mode change (C. T. Russell, private communication). Other than the period of this artifact in the data, the B_z model fit is generally quite good. Note also that the "dipolarization" of the magnetic field at the ISEE location commenced at ~ 0110 UT with the beginning of a substantial increase in the B_z component. However, the Bx component did not simultaneously decrease in magnitude, but rather it actually increased in magnitude until ~ 0119 UT. In general after the substorm onset, the standard Tsyganenko representation did not provide a good fit to the data. It is seen in Fig. 6 that the model fit to the B_y component also was not particularly good during the growth phase: this may be due to significant large-scale current systems in the near-tail during this time (Pulkkinen et al., 1991; 1992). On the other hand, it may be that the large excess B_y is due to IMF penetration although the size of the B_y effect seems too large for this to be the explanation. It could also be the case that the entire Region 1 - Region 2 system is enhanced due to the strong geomagnetic activity. After the substorm onset, the model fit of B_y is (perhaps surprisingly) much better.

In Fig. 7, it is found that the modified Tsyganenko model fit provides a good representation both of the magnitudes and the temporal trends of the B_x and B_z field components seen at GOES-5 between 0000 and 0110 UT on 3 May. The principal discrepancy between the data and the fit seems to be a 10-20 nT underestimate of the B_x component in the modified model. As was the case for ISEE-1, the B_y component is not particularly well-modeled during the growth phase, as noted above, perhaps owing to field aligned currents not accounted for in either the standard Tsyganenko, or the modified, representations.

Fig. 9 shows the model fits to the GSM components of the magnetic field observed at SCATHA. The imperfect removal of the spacecraft spin-modulation from the field measurement is most evident in the B_z component. However, the modified Tsyganenko representation fits the lower envelope of the B_z component very well throughout the growth phase,and the B_x fit is also quite good. As in the cases of ISEE-1 and GOES-5, however, the model fit does not represent the absolute magnitude of B_y very well at SCATHA, even though the general temporal trend in the data is replicated. Note that the sense of the B_y discrepancy is the same as at ISEE-1 on the opposite side of the current sheet. This implies that the B_y is caused either by externally imposed perturbation (inferred to be a positive IMF B_y) or by a strong, large-scale field-aligned current flowing poleward of SCATHA but equatorward of ISEE-1.

Thus, using the methods of Pulkkinen (1991) and Pulkkinen et al. (1991), it has been possible to use multi-spacecraft observations throughout the (pre)midnight sector to arrive at a reasonable model of the time-varying magnetic field during the substorm growth phase. This model provides a global representation of the nightside region at any given time. As would be suggested by the large temporal changes in the field components between 0000 UT and 0110 UT in Figs. 6, 7 and 9, the modified model is extremely important if one wishes to have a realistic "snapshot" of the magnetic field at some arbitrary point during the growth phase sequence.

The degree to which the modified field model departs from the standard Tsyganenko representation at the end of the 3 May growth phase is illustrated in Figure 10. Fig. 10a shows the unmodified Tsyganenko (1989) field line traces for $Kp \geq 5^-$ in the midnight meridian plane. Fig. 10b is a similar plot, but it shows the field line traces in the meridian at 146° longitude (i.e., the approximate longitude of ISEE at 0112 UT). In contrast, Figs. 10c and 10d show the field line configurations computed at 0112 UT in the modified field model. Fig. 10c shows the noon-midnight meridian and Fig. 10d shows results for $\phi = 146°$. The dashed lines near the equatorial plane in Fig. 10 show the approximate extent of the current sheet region in each case, and the labelled dots show the projections of the several spacecraft onto the respective meridian planes. The remarkable field line stretching in the modified model compared to the standard Tsyganenko plot is quite striking throughout the entire inner tail region.

A significant measure of the magnitude of change implied by the modified model compared to the standard Tsyganenko representation is the integrated cross-tail current at a given distance down the tail. Figure 11 shows the integrated current K(mA/m), in the $\phi = 146°$ meridian. The dashed line shows the value of K as a function of radial distance for the standard Tsyganenko model ($Kp \geq 5^-$). The solid line is the equivalent value of K for the modified model as illustrated in Fig. 10. Note that the modified model shows peak cross-tail currents inside of geosynchronous orbit that are nearly twice as great as the standard model. Such peak currents clearly are necessary during strong growth phases (Kaufmann, 1987; Baker and McPherron, 1990).

Expansion Phase Onset

Ground magnetic and auroral imaging data discussed above allow us to specify with considerable confidence that the substorm expansion phase onset occurred at 0111 UT. As shown in Figs. 6 and 7, the ISEE-1 and GOES-5 data, respectively, tended to support this as the earliest probable onset time. Careful examination of the ISEE and GOES magnetic field data show that, in

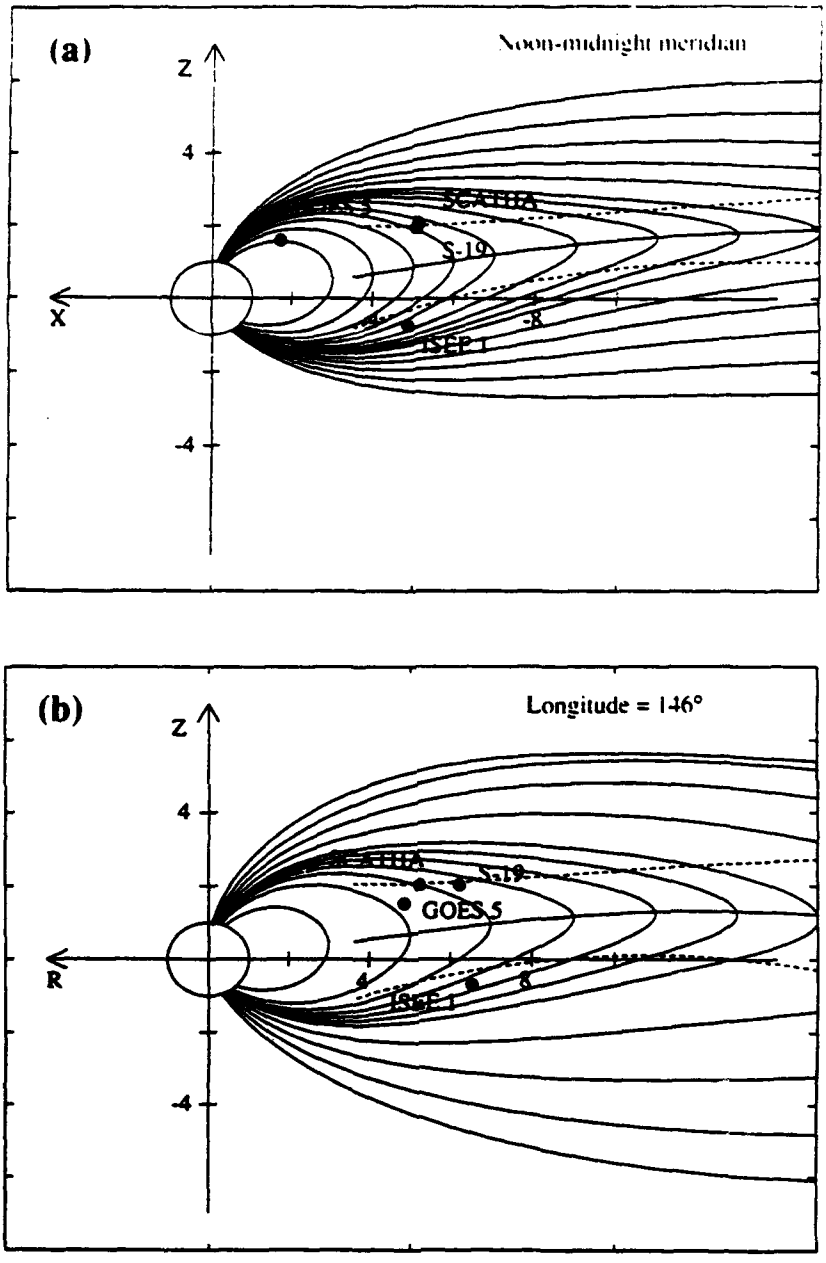

Fig. 10. Meridian plane projections of magnetic field lines. (a) Midnight meridian projection of the Tsyganenko (1989) model field (for Kp ≥ 5). (b) Similar to (a) but for longitude = 146° (~ 21 LT). (c) Similar to (a) but for the modified time-dependent model described in the text. The plot is for 0112 UT on 3 May 1986. (d) Similar to (c) but for ~ 21 LT.

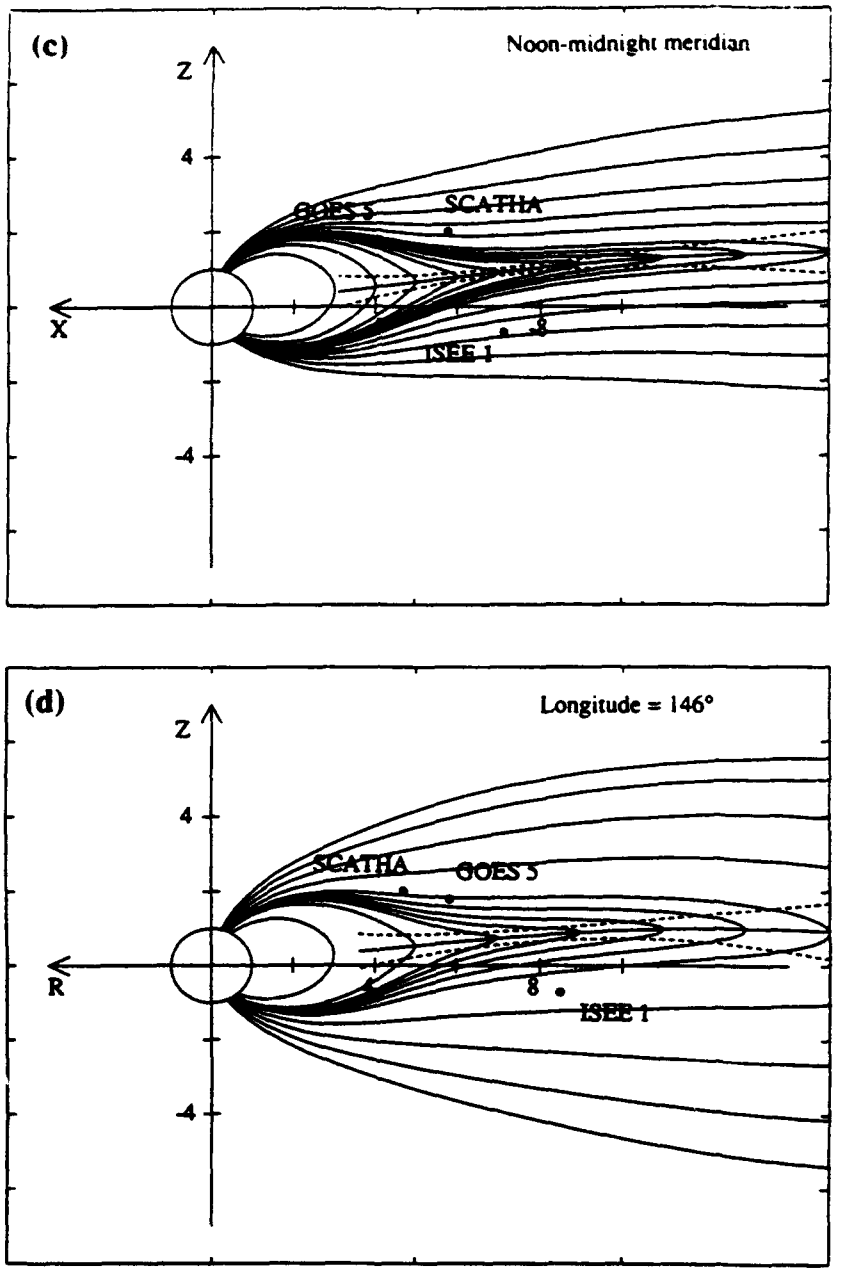

Fig. 10. Meridian plane projections of magnetic field lines. (a) Midnight meridian projection of the Tsyganenko (1989) model field (for Kp ≥ 5). (b) Similar to (a) but for longitude = 146° (~ 21 LT). (c) Similar to (a) but for the modified time-dependent model described in the text. The plot is for 0112 UT on 3 May 1986. (d) Similar to (c) but for ~ 21 LT.

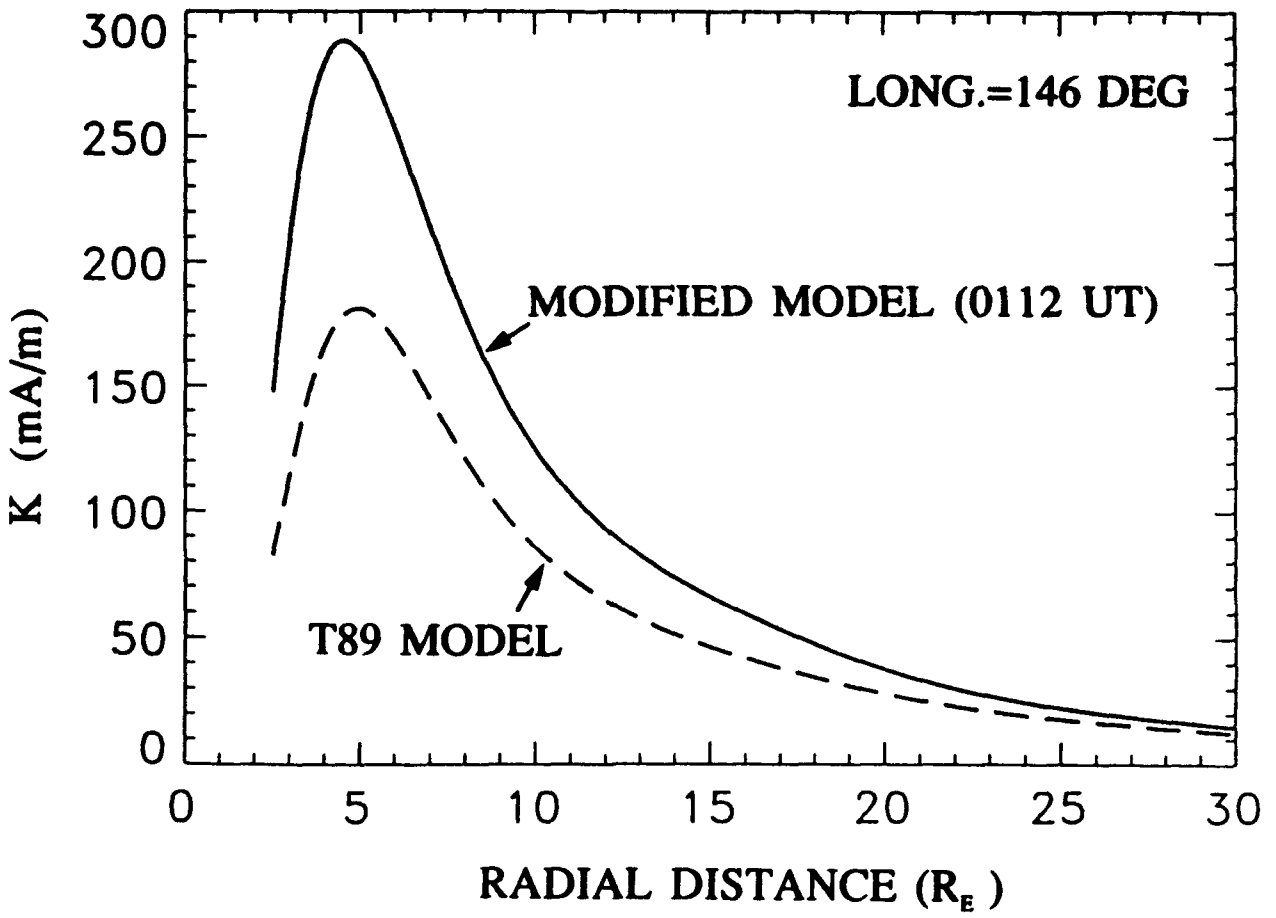

Fig. 11. Integrated cross-tail currents as a function of radial distance down the magnetotail. The dashed line is for the Tsyganenko (1989) mode with Kp ≥ 5⁻, while the dotted line is for the modified model of Pulkkinen et al. (1991) as described in the text.

reality, it was the B_z component at each spacecraft that showed the most prompt signature, with the B_x, B_y, and plasma signatures being somewhat more delayed and variable in their response. The B_x component at ISEE-1 did not diminish in magnitude until ~ 0119 UT, and the plasma ion temperature increased markedly at about the same time. The plasma flow speed measured by ISEE also increased as the ion temperature increased.

At GOES-5, the B_z component increased slightly right at 0111 UT. However, B_y became less negative later (~ 0113 UT) and B_x actually became larger until nearly 0115 UT. A more complete "dipolarization" of the field at GOES did not occur until nearly 0120 UT. In Fig. 8, it is seen that the recovery of energetic electron fluxes above background levels was delayed by several minutes relative to the substorm onset at 0111 UT. Indications in Fig. 8 are that S19 saw a beginning of > 30 keV electron flux recovery at ~ 0115 UT. Note also, however, that a fresh "injection" of energetic electrons (e.g., Baker et al., 1978) well above the predropout flux level did not occur until ~ 0124 UT, a delay of 13 min from the expansion phase onset as identified by intensification in the ground magnetometer records.

The case of SCATHA is interesting also in its substorm timing sequence properties. As noted for ISEE and GOES, the B_z component at SCATHA showed the most prompt response to the substorm onset. Because of the spin-modulation signal in B_z it is hard to be precise, but it appears that SCATHA measured an increase in B_z at ~ 0112 UT. As noted also for the other spacecraft, however, B_x continued to increase at SCATHA (in fact, the rate of increase was enhanced for a time) after 0111 UT and B_x did not decrease substantially until at least 0117 UT. This was also about the time that > 30 keV ion fluxes at SCATHA recovered from their growth phase (dropout) levels.

Thus, the indications are that the B_z component strengthened promptly, but weakly, throughout most of the (pre)midnight sector shortly after the 0111 UT auroral brightening observed by Viking and DE-1. There were also reasonably prompt signatures seen in the B_y components measured at various near-tail spacecraft, but B_x components were large and persisted for several minutes after the onset time at the various spacecraft locations. This suggests that there was not an immediate, fully-developed current wedge formation throughout the midnight sector in this case. Rather, there was a more gradual and progressive development of the current wedge system which depended sensitively on the observing spacecraft position.

Magnetic Mapping of the Substorm Current Wedge

Using the modified Tsyganenko model described above, we have demonstrated that a realistic global representation of the near-tail field has been developed for the entire growth phase of the 3 May substorm event. In particular, the model provides a good description of the magnetospheric field configuration right at the time of the expansion phase onset (~ 0111 UT). Fig. 10 shows the model meridional field line configuration for this case at two different longitudes, as we have previously described.

To provide a different view, the top panel of Figure 12 shows the projections of selected model field lines onto the equatorial (X-Y) plane at the end of the growth phase. The field lines in Fig. 12a were chosen to be at constant magnetic latitudes and traces were done at one-hour longitude intervals in the night sector. Two sets of field lines were mapped, one set emanating from 59° latitude and the second set emanating from 61° latitude. As seen in the figure, the 59° field lines cross the equator near synchronous orbit at ~ 21 LT and ~ 03 LT, but extend to $\geq$ 15 R_E nearer local midnight. The 61° field lines extend to ~ 15 R_E away from midnight, but extend to ~ 30 R_E (i.e., well beyond the scale of Fig. 12) near the midnight meridian.

The auroral imaging data, which showed that the onset took place between 0110:29 and 0112:10 UT, and ground-based magnetic records show that the substorm onset occurred in a narrow region near 21 MLT. The positions of several relevant near-tail spacecraft at this time are shown projected onto the X-Y plane in Fig. 12. We also show the meridian of substorm onset at 0111 UT: This line was seen to be between ISEE-1 and GOES-5, but was closest to the ISEE meridian.

The analysis of substorm expansion features seen at the various near-tail spacecraft described in the previous section shows that the substorm disturbances expanded eastward and westward in a progressive way. By 0112 UT ISEE-1 and GOES-5 had definitely begun to observe evidence of the substorm current wedge (SCW). This is illustrated in Fig. 12b. (For reference, we repeat as dashed lines in each panel of Fig. 12 the field line projections calculated at the end of the growth phase.) By 0115 UT, S19 had seen a dipolarization of the magnetic field and a recovery of energetic electron fluxes. This suggests that the current wedge had, by ~ 0116 UT, spread beyond the longitudes of both S19 and GOES-5; this is shown in Fig. 12c. Finally, by 0120 UT all of the inner tail spacecraft, including SCATHA (~ 0117 UT), had observed the current wedge formation. Thus, as shown in Figure 12d, by ~ 0120 UT the region of substorm disturbance and SCW formation was apparently some five to six hours wide in local time.

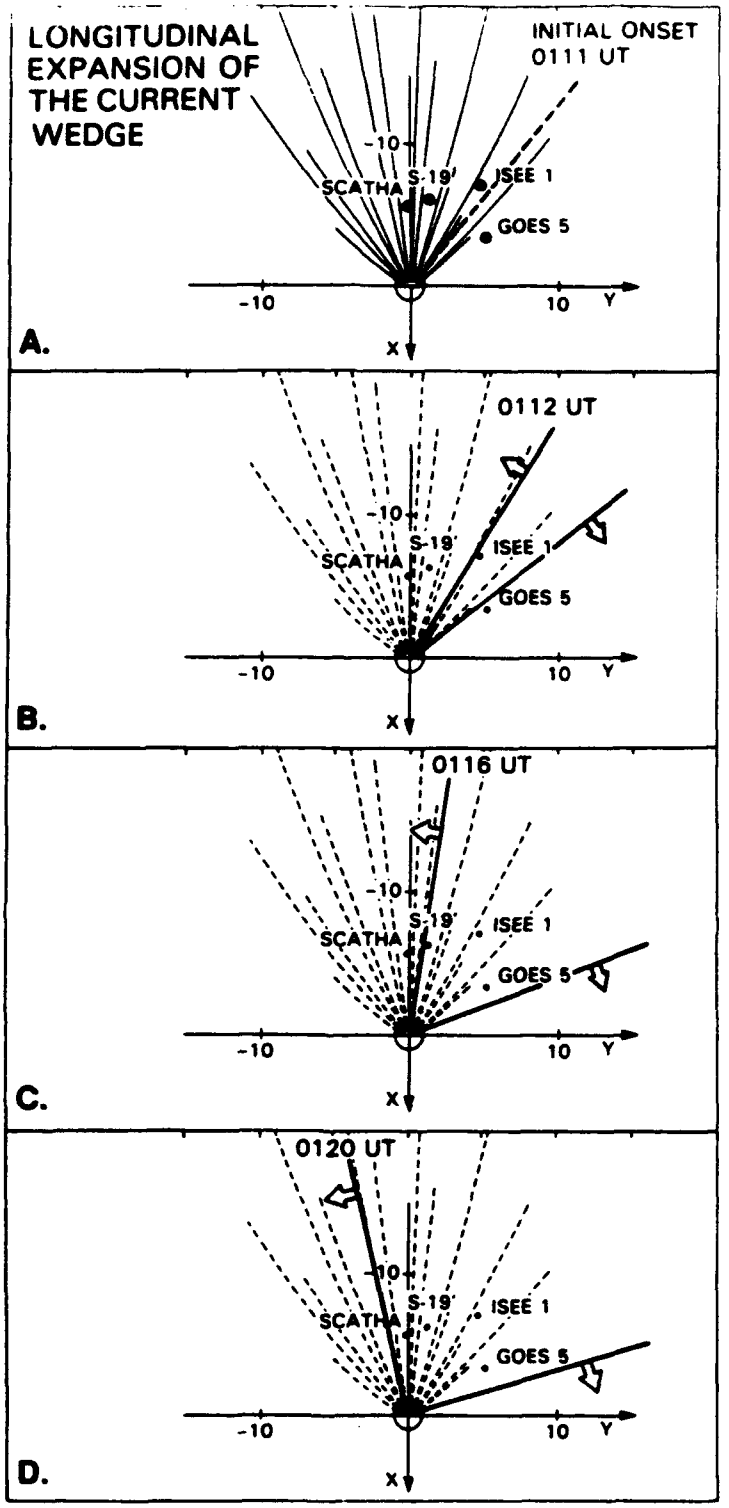

Fig. 12. (a) A projection of field lines onto the equatorial plane in the modified magnetic field model discussed in the text. Two sets of field lines are shown, one set emanating from 59° magnetic latitude and the other from 61° magnetic latitude. The heavy dashed radial line shows the substorm onset meridian at 0111 UT. Panels (b) - (d) show the subsequent longitudinal spread of the substorm disturbance as seen by the several high-altitude spacecraft.

The spreading of the substorm onset disturbance is, in reality, a complex 3-dimensional problem. In addition to the longitudinal current wedge expansion shown in Fig. 12, there also would be massive reconfiguration of the current sheet and the latitudinal extent of magnetic flux tubes within the region of the SCW. In Fig. 13 we illustrate the latitudinal expansion of the substorm disturbance. Fig. 13a is a repetition of the modified Tyganenko state at $\phi = 146°$ shown previously in Fig. 10d. Again, we show the several spacecraft positions projected onto the meridian plane. If we take the times of major reconfiguration of the B_x component at each spacecraft position to be the time of current sheet expansion, we would conclude that not until ~ 0120 UT (Fig. 13d) had the latitudinal expansion fully reached SCATHA, GOES, or ISEE-1. The sequence shown in Figs. 13b and 13c is consistent with the observations described in relation to Figs. 6-9 above.

Magnetic Mapping of Expansion Auroral Features

Fig. 14 is a detail of the DE-1 auroral image taken beginning at 0113 UT on 3 May. It is plotted in geographic coordinates and shows the large region of brightened auroras that were evident in Fig. 2 between 21 MLT and local midnight. This auroral activity appeared suddenly after the 0111 UT onset and was not present in the prior DE-1 image at 0105 UT (see Fig. 2). Note that the most intense region of auroral brightening in Fig. 14 was actually near ~ 60° magnetic latitude and this part of the image was scanned within the time interval ~ 0115-0117 UT.

Fig. 15 is a sequence of detailed images from Viking in a similar format to Fig. 14. It shows the 0112:10 UT, 0112:50 UT, and 0118:32 UT images of the brightening and expanding auroras. These images make clear that the initial auroral brightening occurred at quite low latitude, while there were bright auroral features more poleward that were eventually enveloped by the spreading auroral expansion. There also were diffuse auroral luminosity signatures in the premidnight sector extending even further poleward. The discrete structure at the poleward edge of the auroral feature at ~ 0113 UT is close to the region where the strongest electrojet currents were inferred to flow. We infer that the onset of this substorm occurred quite close to the Earth since the aurora brightened so far equatorward (Murphree et al., 1991; Murphree et al., 1992).

Using the modified magnetic model described previously, we can utilize the magnetic field configuration inferred right at the end of the growth phase to map the auroral features out to the magnetic equatorial plane. Obviously, there is some limitation to the correctness of this mapping since after substorm onset the global field begins rapidly to reconfigure itself. However, for a brief period right at the expansion phase onset time, this approximation should be quite valid. (We

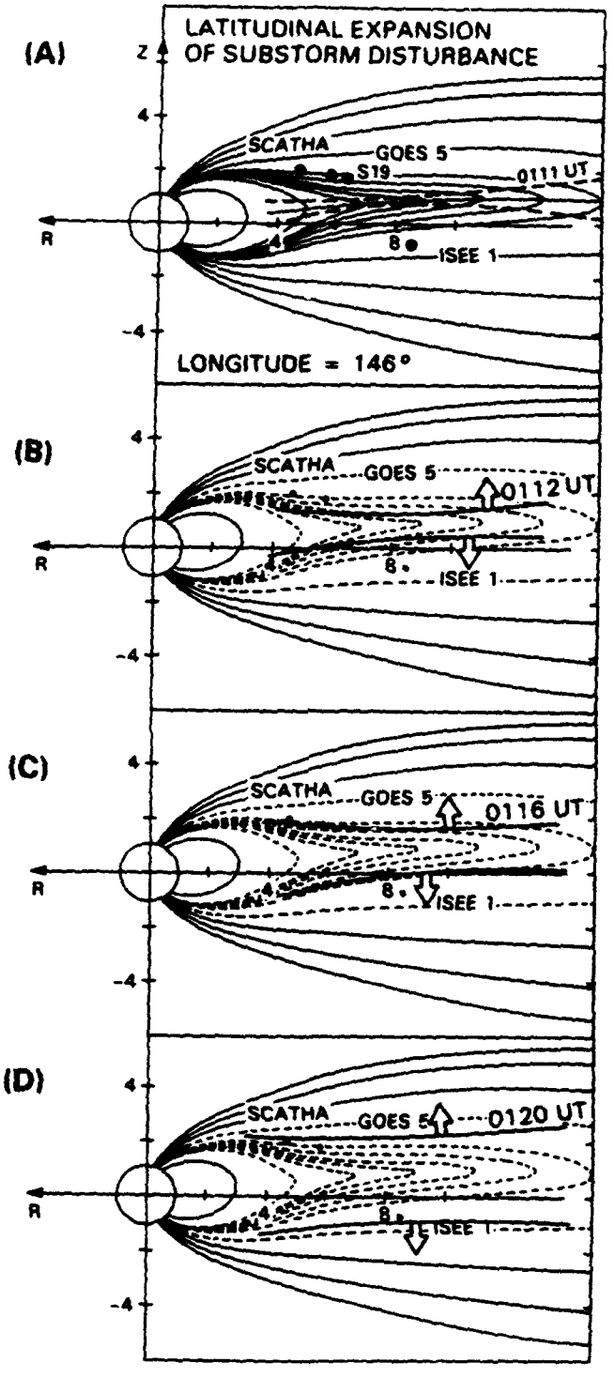

Fig. 13. (a) A plot of the model magnetic field and current sheet in the $\phi = 146°$ meridian (similar to Figure 10d) for 0111 UT on 3 May. Panels (b) - (d) show the apparent latitudinal expansion of the substorm disturbance with time after the onset.

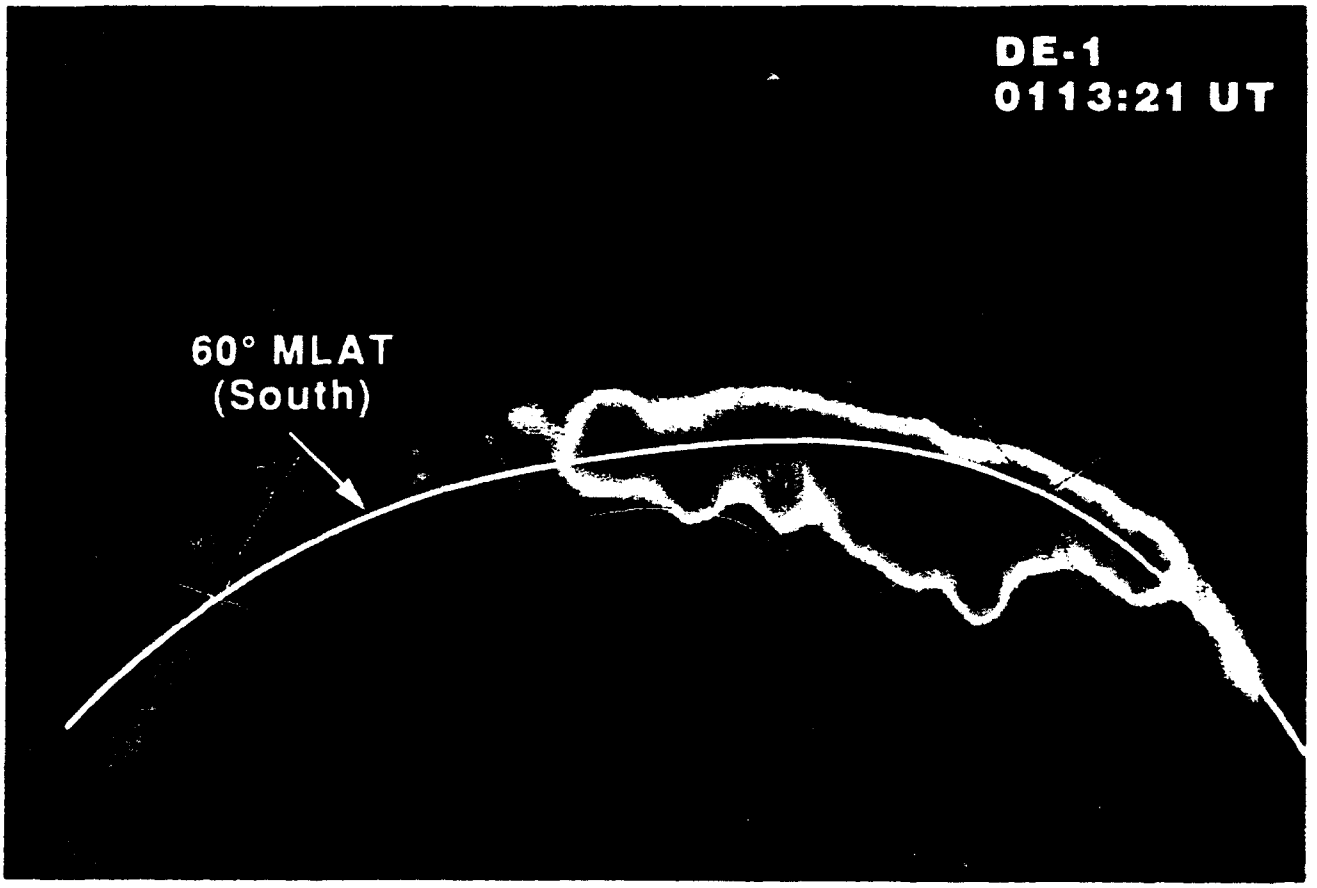

Fig. 14. A detail of the DE-1 auroral image acquired beginning at 0113 UT on 3 May 1986. Isointensity information in this geographic projection was used for model mapping out to the magnetic equator.

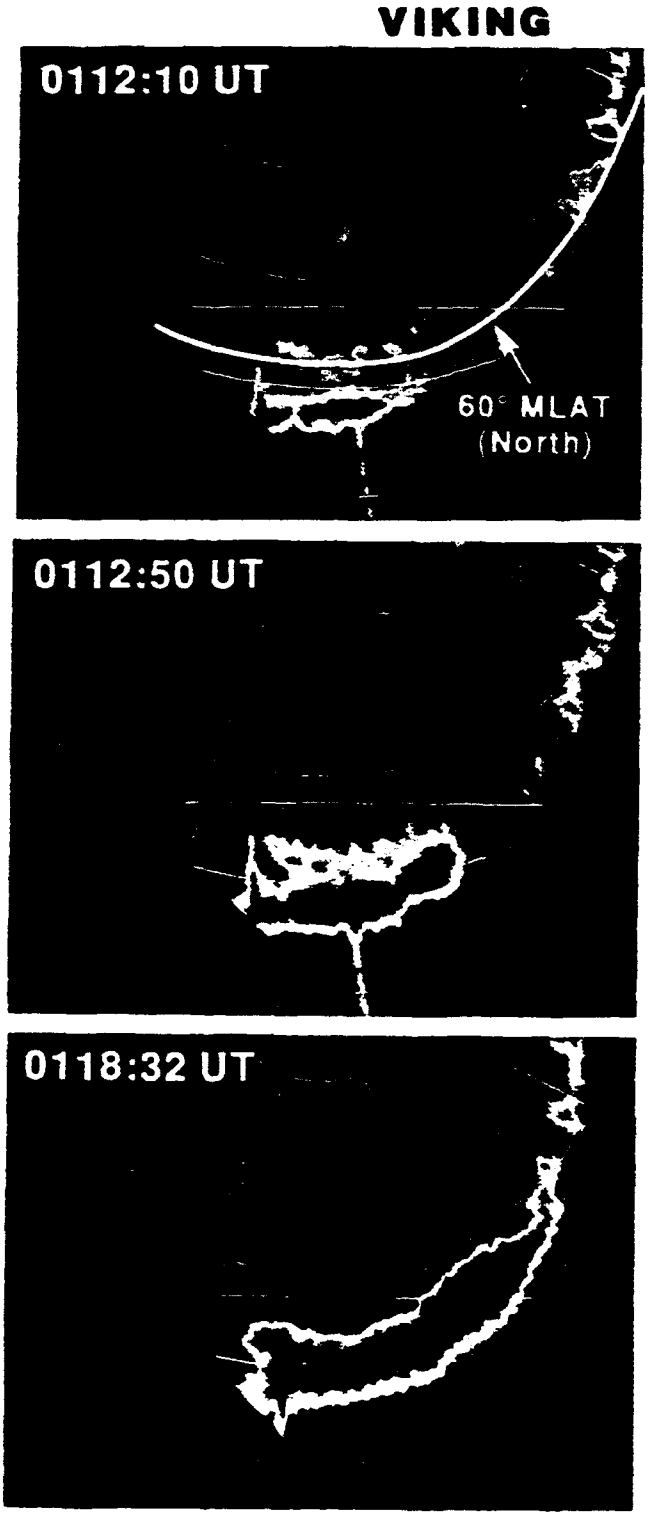

Fig. 15. A detail of the Viking auroral images acquired at 0112:10 UT, 0112:50 UT, and 0118:32 UT on 3 May 1986. As for Fig. 14, the isointensity contours delineating the auroral arc regions associated with the initial substorm onset were used to map features out to the magnetic equator.

also assume here that parallel electric fields do not drastically affect the validity of magnetic mappings right at the onset time.)

For both the DE-1 image (Fig. 14) and Viking image (Fig. 15) we have determined the geographic contour of the brightened auroral region centered at ~21 LT and at $\leq 60^\circ$ MLAT. This intensity contouring traces the outer fringes of the respective auroral features at constant intensity as measured by Viking in the northern hemisphere and by DE-1 in the southern hemisphere. These geographic contours were determined for both the poleward and equatorward edges of the brightened auroral features at ~1° intervals of longitude. Obviously, the DE-1 image (acquired over an 8-min interval) represented a much more expanded auroral configuration than did the 1-s Viking snapshot.

In Fig. 16a we show equatorial projections for two different DE-1 isointensity contours. The inner mapped region corresponds to about twice the auroral luminosity of the outer region. (In Fig. 14, these regions correspond, respectively, to the outer edge of the red false color region and to the outer edge of the yellow region.) The mapped contours extend very close to the Earth in the premidnight sector (5-10 R_E), but extend far down the tail (~ 40 R_E) near midnight. In comparison, Fig. 16b shows the mapping of the three Viking images taken at 0112 UT, 0113 UT, and 0118 UT (as shown in Fig. 15). The three different shadings denote the mappings at different times, with the darkest shaded region corresponding to the initial auroral brightening seen by Viking at 0112 UT. Note that it maps to well before midnight and quite close to the Earth. The larger and lighter shaded regions in Fig. 16b show the subsequent spreading of the aurora seen by Viking. The lightest shading covers the largest area corresponding to the mapping of bright aurora for the latest time at 0118 UT. The spreading is largely eastward (toward midnight). This result is quite consistent with the results shown in Fig. 12. Note that the Viking projected auroral region for 0118 UT in Fig. 16b is rather comparable in character to the DE-1 projected auroral image in Fig. 16a. Given that DE acquires an image over a period of 8 min, and it began the image collection at 0113 UT, the middle part of the DE image would have been assembled between ~ 0115 and 0117 UT. Thus, this should be reasonably comparable to the 0118 UT Viking image.

In Fig. 16c, we explicitly overlay the ~ 0115-0117 UT DE auroral projection with the 0118 UT Viking projection. Except in the region of local midnight for $-5 \lesssim x \lesssim -15$ R_E, there is rather good correspondence between the two projections. In the near-tail, near-midnight region, Viking shows mapped brightening not present in the DE image. Whether this is a true north-south asymmetry or is due to time-aliasing in the DE data is not clear. Otherwise, there appears to be remarkably good conjugacy between the DE and Viking images at comparable times in this case.

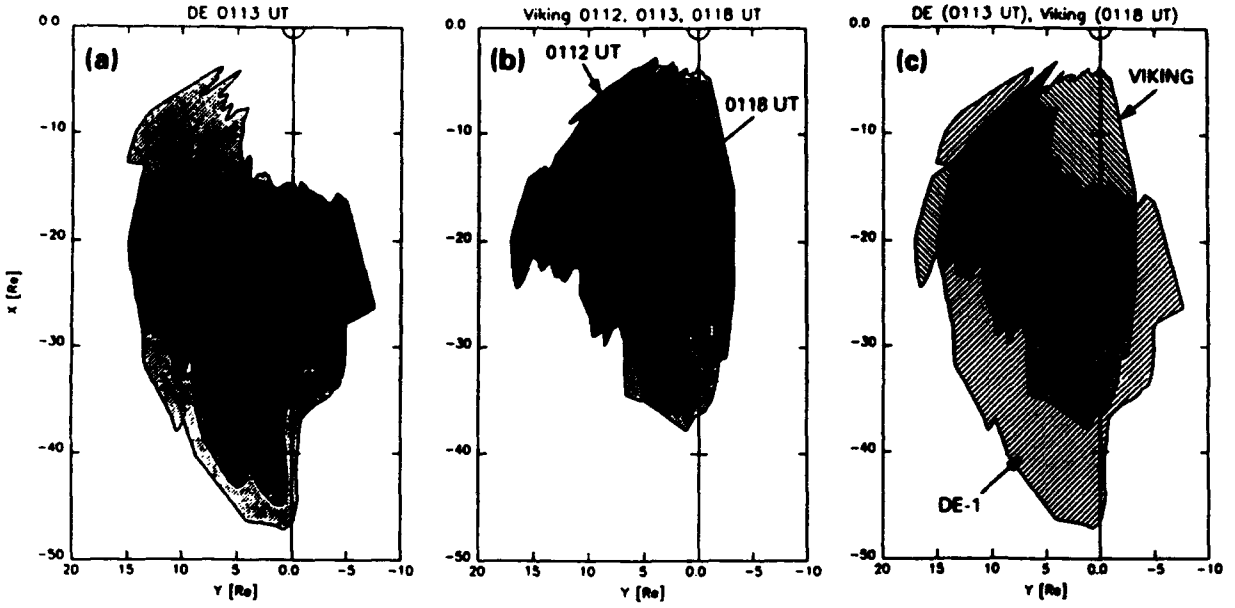

30

Fig. 16. (a) A mapping of the DE-1 auroral image of Fig. 14 to the equatorial plane using the model of Pulkkinen et al. (1991). (b) Similar to (a) using the Viking image sequence of Fig. 15. (c) An overlay of the DE-1 and Viking (0118 UT) mapped images.

Thus, the effect causing the discrepancy between the model field Y-component and observed B_y at both SCATHA and ISEE-1 has the same sense for a large portion of the tail. If this were not true, then the mappings of Fig. 16 would not show conjugacy of auroral features.

The global field model used here allowed Pulkkinen et al. (1991, 1992) to study the particle motion in the changing growth phase field geometry. Earlier, Büchner and Zelenyi (1987) studied particle trajectories during current sheet traversals assuming a parabolic field configuration. It was concluded that stretching of the tail field during the growth phase leads to chaotization of electron motion. The degree of chaotization was described by the parameter $\kappa = (B_n/B_0)\ (\lambda/\rho e_0)^{1/2}$ where λ is the current sheet thickness and ρe_0 is the electron Larmor radius in the lobe field B_0, and the chaotic domain is determined by $\kappa < 3$. When the scattering becomes strong enough ($\kappa \leq .6$), Büchner and Zelenyi argued that the ion tearing instability is triggered at substorm onset.

Pulkkinen et al. computed κ from the modified Tsyganenko field model, using D(X,Y) as λ, the parallel field component 5 R_E above the current sheet as B_0, and the field component normal to the current sheet as B_n. They showed the contours for constant κ for 1 keV electrons were found to be adiabatic throughout the tail, and the unstable region for energetic electrons ($\approx$ 10 keV) was small and located around 20 R_E. In the modified model, however, the enhancement of the currents induced chaotic motion for thermal electrons in the region between ~8 and ~15 R_E a few minutes before the onset, and the critical value for the instability $\kappa = 1.6$ was reached shortly after that within a slightly small region. This chaotic region falls well within the region shown in Fig. 16 where the aurora initially brightened at substorm onset.

Distant Magnetotail Observations

A final set of observational information for the 0111 UT substorm was available from IMP-8 at ~33 R_E geocentric distance in the magnetotail. Hot plasma ($\geq$20 keV ions and electrons), energetic ions (0.29-0.5 MeV), energetic electrons (0.22-0.5 MeV), and magnetic field measurements for the period 0000-0300 UT on 3 May are plotted in Fig. 17. The IMP-8 position in GSM coordinates is shown along the bottom of the figure.

The $\geq$20 keV channel shown in the upper panel of Fig. 17 (probably dominated mostly by suprathermal electrons) clearly delineates the tail lobe (or fringe regions of the plasma sheet) where hot plasma is virtually absent. These regions were encountered from 0000 until ~0015 UT and from ~0150 to 0235 UT. Another brief lobelike region was approached between ~0050 and 0056 UT. The remaining intervals were times when IMP-8 was rather solidly embedded within the

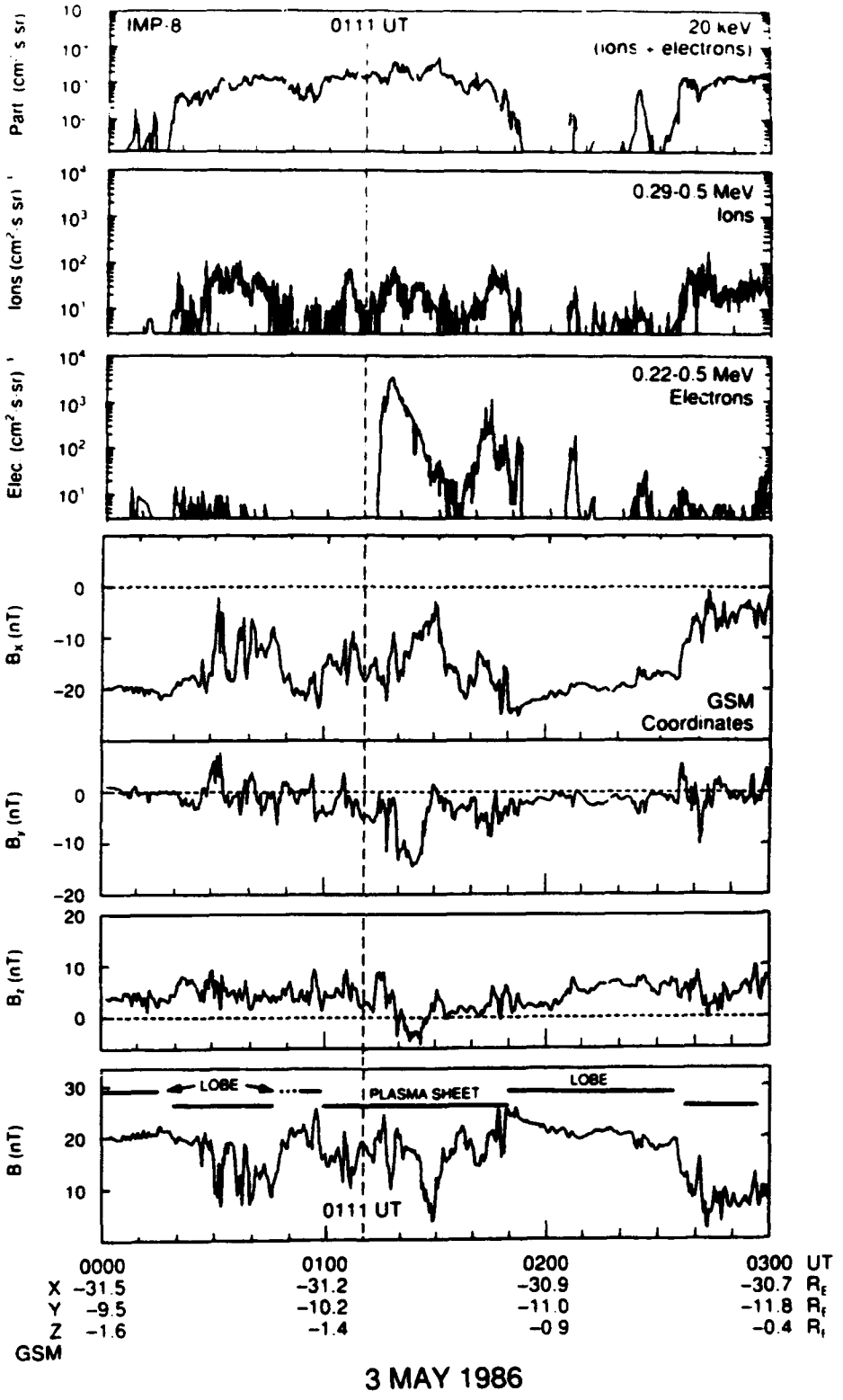

Fig. 17. A summary of hot plasma, energetic particle, and magnetic field data from IMP-8 in the middle magnetotail on 3 May 1986.

distant plasma sheet. These plasma regional identifications are well supported by the magnetic field data in the lower four panels of Fig. 17. In the lobe (or lobelike) regions, B_x was strongly negative being near ~-20 nT. At these times B_y was ~0 and B_z was slightly positive (~4-6 nT); these values of the field components are consistent with IMP-8 being in the southern tail lobe. During the plasma sheet encounters, however, $|B_x|$ diminished strongly as, of course, did $|B|$ implying a large diamagnetic effect within the hot plasma region. Note that the 0.29-0.5 MeV ions were generally elevated in flux within the plasma sheet, but were absent in the lobes (Lui et al., 1984).

There are indications that the lobe field strength at IMP-8 increased during the course of the previously identified growth phase (i.e., 0000 to 0111 UT). At 0000 UT, IMP-8 was clearly in the tail lobe and B was 20 nT. At ~0056 UT, IMP was back briefly very near the tail lobe (note the strong B_x and reduced particle fluxes); at that time, B was at least 25 nT. This increase of B by $\geq$25% is consistent with growth phase enhancements in the lobe studied previously (e.g., Baker et al., 1981; Schindler et al., 1989).

The most striking features of the present IMP-8 data occurred beginning at ~0113 UT. At that time there was a sudden factor of 10^4 increase in the flux of >220 keV electrons. Concurrently, B_z first rotated northward by several nT and then by 0119 UT it rotated substantially southward. This was the only episode of southward B_z seen on this entire day in the magnetotail. The occurrence of enhancements of very energetic electrons and southward B_z in the plasma sheet has been associated in many previous cases (e.g., Baker and Stone, 1976, 1977; Sarris et al., 1978) with magnetospheric substorms. The occurrence of negative B_z in such cases has been taken as evidence of near-Earth neutral line formation and plasma sheet reconnection processes (Baker and Stone, 1977; Frank et al., 1976; Hones, 1977).

The great enhancement of the mildly relativistic electrons seen in Fig. 17 occurred beginning at ~0113 UT, i.e., about 2 minutes after the identified substorm onset nearer Earth. There was a brief indication of tailward streaming of the electrons early in the flux enhancement (data not shown) which may indicate open, reconnected field lines (Baker and Stone, 1976). However, during the period of strongly southward B_z, the electron flux was rapidly diminishing and the particle distributions were nearly isotropic. This isotropy of the electrons may be taken as an indication of closed field line structure (Baker and Stone, 1976). Southward plasma sheet field configurations with isotropic energetic electrons have been seen previously within the distant magnetotail and associated with tailward propagation of plasmoids (Scholer et al., 1984; 1985). The large negative B_y during the electron enhancement and the southward B_z may indicate an edge

effect as the field drapes around a retreating plasmoid, or it may indicate more of a "flux rope" structure rather than a plasmoid per se (Hughes and Sibeck, 1987). In either case, there was clearly a significant dynamical event in the mid-magnetotail region that occurred shortly after the identified substorm onset.

Discussion and Interpretation

In the present study, we have had available a large array of ground-based and satellite data with which to study the growth, expansion, and early recovery phase of an exceptionally intense substorm event. The expansion phase onset was well-identified both by auroral imaging experiments and by ground magnetometers to be at 0111 UT. The onset appeared to occur in a narrow longitudinal sector (e.g., Nagai, 1982; Nagai et al., 1983) and the activity then spread progressively eastward and westward for some 10-20 min. Both the auroral imagers and a suite of well-placed (near-)geostationary spacecraft established the longitudinal expansion of the current wedge away from its initial site near 21 MLT.

The rate of the eastward expansion of the current wedge can be readily estimated from the satellite measurements as summarized in Fig. 12. From that diagram, using the longitudinal spreading of the disturbance toward local midnight, we can determine that the eastward edge of the reconfiguration moved from 21 LT to ~ 01 LT between 0111 UT and ~ 0120 UT. Taking a characteristic equatorial radial distance of 7 R_E, we have an equatorial angular spread of ~60° and an arc length ($2\pi R/6$) of $s = 4.7 \times 10^4$ km. The average expansion speed over the 9-min interval is then $s/\Delta t$ = 86.5 km/s. At ionospheric altitudes near 60° MLAT, this expansion rate would correspond to ~ 6.3 km/s. Such a value seems quite consistent with the rapid eastward spreading seen in the imager data. Ground-based and high-altitude satellite data all suggest that the westward expansion of the substorm activity in this case was less extensive and was less rapid (by perhaps a factor of 2) compared to the eastward expansion. (The DE-1 image at 0129 UT, however, shows greatest expansion into the evening sector, while the morning expansion picked up later.)

Perhaps the most intriguing aspect of this event was the extreme taillike stretching of the magnetic field very close to the Earth late in the substorm growth phase. This feature of strong substorms has received considerable attention in the literature recently (Kaufmann, 1987; Baker and McPherron, 1990; Baker and Pulkkinen, 1991). It is clear that late growth phase field distortions require a quite thin, radially localized cross-tail current sheet extending inward at least to the vicinity of geosynchronous orbit. As shown by the modeling presented in this paper and in other recent work (Sergeev et al., 1990; Pulkkinen et al., 1991, 1992), the inclusion of such thin

current sheets can replicate the observations very well. The question left unanswered by such empirical modeling, of course, is what physical processes lead to such an extreme configurational situation.

Baker and McPherron (1990) suggested that a slight departure from the "standard" substorm model could possibly explain the puzzle of late growth phase observations. They proposed that rather than having a magnetic neutral line form suddenly right at substorm expansion phase onset, instead the neutral line might form some 10-20 minutes before the substorm onset. They suggested that this neutral line would, indeed, form at the geocentric distance of 15-20 R_E in the nightside magnetotail (as in the standard model), but they speculated that in this early stage the neutral line would form on the closed field lines of the central plasma sheet. In this relatively high-β region, the Alfvén speeds in the reconnection inflow regions would be small (~100 km/s) and the effective reconnection rates would be low (Vasyliunas, 1975).

An important effect of the near-Earth neutral line in the standard substorm model is to "disrupt" and divert cross-tail current from the plasma sheet into the ionosphere to form the current wedge (Atkinson, 1967; McPherron et al., 1973). Baker and McPherron (1990) suggested that the neutral line would initially divert cross-tail current Earthward within the plasma sheet because of the relatively low ionospheric conductivities at that stage of the growth phase and because of the large inductances required to set up field aligned currents (FACs) to the ionosphere. Thus, Baker and McPherron proposed that for some extended period, the initial neutral line would reconnect closed plasma sheet field lines rather slowly (hence not changing the basic field configuration drastically) and would divert cross-tail current toward the inner edge of the plasma sheet (without yet forming a substorm current wedge or strong FACs). A principal effect of this scenario would be for the weak, growth-phase neutral line to drive the formation of the intense cross-tail current sheet that is observed so prominently near the Earth toward the end of the growth phase.

In Fig. 18 we illustrate the situation that appears to apply in the case under study right at the end of the substorm growth phase and just at the beginning of the expansion phase. Following the suggestion of Baker and McPherron (1990), we propose that an initial X-line (and accompanying O-line) begins to form at two to three times the geosynchronous orbit distance. As discussed above, this neutral line would form in the hot central plasma sheet and would begin weakly reconnecting closed flux tubes. This would form tailward "magnetic islands," but these would be confined and restrained by the overlying (still-closed) plasma sheet flux tubes. Earthward of the X-line, the current that had been flowing within the neutral line region would be diverted into an increasingly confined radial range giving rise to the very high current densities illustrated in Fig.

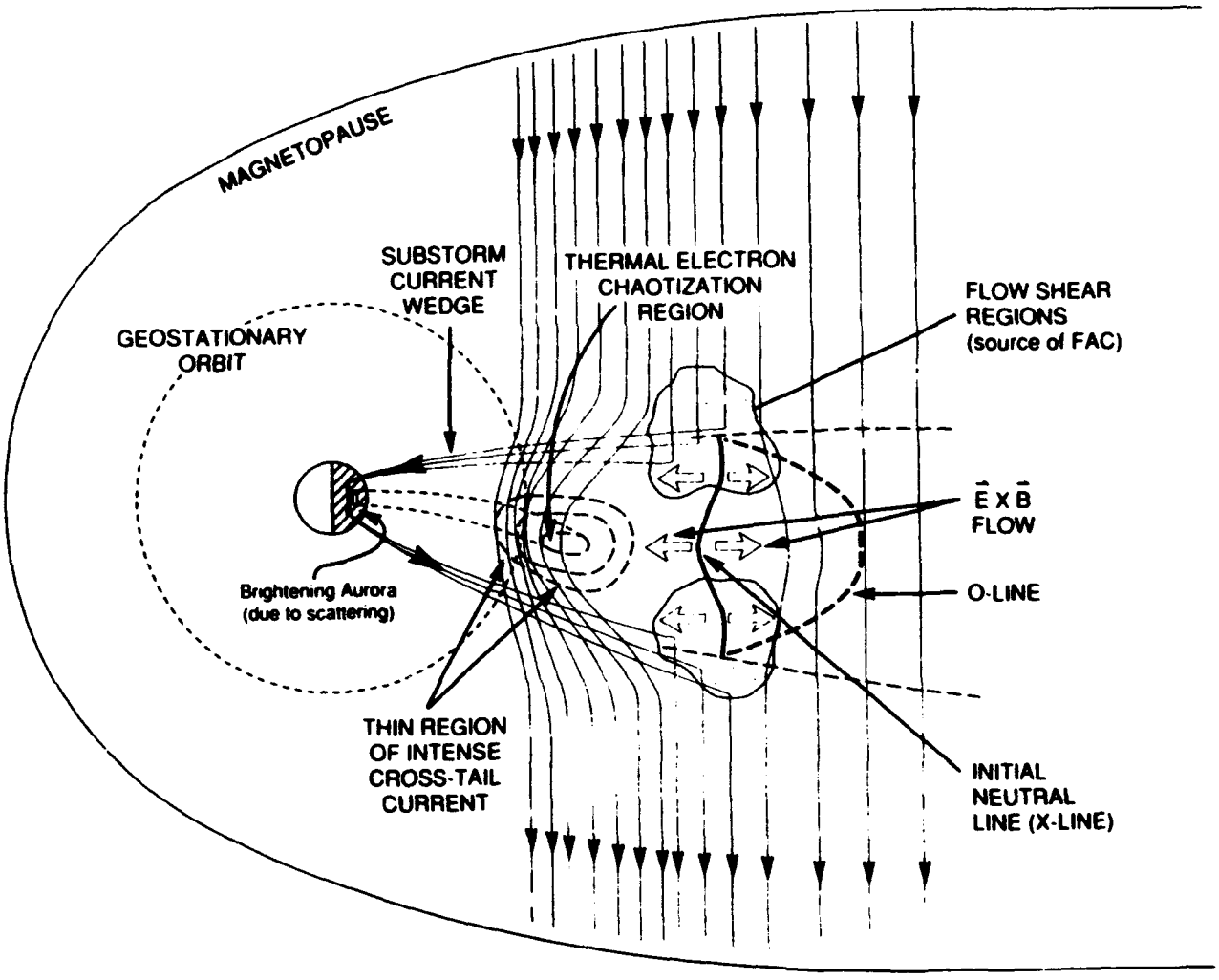

Fig. 18. A schematic diagram of the near-Earth plasma sheet and cross-tail current sheet region during the late growth phase (and very early expansion phase) of the 0111 UT substorm on 3 May 1986.

18. These concentrated current flow lines near geostationary orbit would constitute the thin current sheet we have invoked above to explain the taillike stretching at GOES, ISEE, and SCATHA.

The extreme taillike field stretching that occurs close to the Earth implies that the current sheet (and field reversal region) in this area is very thin in the north-south sense (Sergeev et al., 1990; Pulkkinen et al., 1991, 1992). Such thin current sheets have profound effects on the particle confinement properties of the tail magnetic fields (e.g., Mitchell et al., 1990) and, in fact, considerable scattering of particles can occur in these thin current sheets as the field line radius of curvature becomes comparable to the particle gyroradii (Büchner and Zelenyi, 1987; 1989). Pulkkinen et al. (1991; 1992) have studied the ion and electron "chaotization" which occurs in these cases of very thin current sheets using a temporally evolving global magnetic field model. The model results suggest that in most substorm cases studied, including the 0111 UT substorm under investigation here, the current sheet became so thin that the motion of even thermal ($\approx$ 1 keV) electrons became strongly chaotic right at the end of the growth phase. Moreover, Pulkkinen et al. showed that the region of initial and maximum electron chaotic motion mapped closely to the region of first auroral brightening (as discussed in association with Figures 15 and 16 above).

Thus, in Fig. 18 we illustrate the κ contours that Pulkkinen et al. found for the thin current sheet regions. The centrally embedded contour would correspond to $\kappa = 1.6$ which would be the region of extreme thermal electron scattering. As discussed previously in this report (and by Pulkkinen et al.), the chaotic electron region occurs remarkably close to the Earth, and it maps closely to the region of initial auroral brightening seen by Viking at 56° MLAT and ~ 21 MLT. This relationship is illustrated in Fig. 18. Chaotization of the electron orbits has been suggested to trigger the tearing instability (Büchner and Zelenyi, 1987), which in turn would lead to partial disruption of the cross-tail current. This would feed electrons into the ionospheric loss cone which, together with parallel acceleration at lower altitudes, may account for the auroral features observed.

A quite striking feature of the 0111 UT substorm on 3 May, however, was that the intense westward electrojet currents at the expansion phase onset did not flow at the low latitudes where the first auroral brightenings occur (56° MLAT). Rather, as shown by the magnetic records from PDB and OTT in Fig. 4, the westward electrojet currents flowed close to, and slightly southward of, PDB at a latitude of ~ 66°. It is quite clear from the OTT (latitude ~ 56°) data (Fig. 4c) that the westward electrojet was far northward of that station until at least 0130 or 0140 UT. Thus, we see a clear demonstration that the auroral brightening occurred in the ionosphere directly above OTT, but the wedge electrojet currents flowed nearly 10° in latitude poleward of this auroral brightening.

In Fig. 18, we suggest a potential explanation of this remarkable set of observations. Again in keeping with the Baker and McPherron (1990) concept, we propose that by ~ 0111 UT on 3 May the magnetic reconnection at the initial X-line had progressed so as to reconnect most of the closed, central-plasma sheet field lines with no obvious auroral signature. At this point the X-line would suddenly begin reconnecting open lobe flux tubes. At this critical point, the reconnection rate would increase dramatically: the Alfvén speed in the inflow region would jump to much higher values (1000-2000 km/s) than for the central plasma sheet and, consequently, the electric fields at the X-line would be much larger (e.g., Axford, 1984). Such a large change in the reconnection rates could have an almost explosive character (Baker and Belian, 1986) leading to very strong energetic particle production. This would also lead to much stronger jetting (ExB flow) away from the neutral line region (Vasyliunas, 1975).

As shown in Fig. 18, we estimate that the neutral line extends over only a limited width of the magnetotail. In fact, it may initially extend over a narrower region than shown in Fig. 18 and may then spread later. We suggest that over most of the plasma sheet width outside of the X-line sector there was only weak earthward plasma flow or perhaps modest tailward flow associated with the growth phase taillike stretching of the field. However, in the longitudinal sector of the neutral line, we expect strong jetting (Earthward or tailward) away from the X-line as open field lines reconnect. At the eastward and westward extremes of the X-line, there would be strong plasma sheet shear flows. These shears would drive strong vorticity development which, in turn, could drive strong field aligned currents (Birn and Hesse, 1991; Hesse and Birn, 1991). Thus, we would suggest that it was the more tailward region, near the original neutral line location, that was the initial and strongest source of the FACs. These would map to much higher magnetic latitudes than would the auroral brightening, as shown in Fig. 18. This could account for the large latitudinal separation of the westward electrojet and the auroral brightening in this very disturbed case. Birn and Hesse attribute current wedge dipolarization in the expansion phase to flux pile earthward of the substorm neutral line. As reconnection progresses from the relatively weak stage in our growth phase scenario to the strong (nonlinear) reconnection of the expansion phase, we would also expect such flux pile up within the current wedge. In our picture, however, the late growth phase is dominated more by cross-tail current diversion than it is by strong plasma flow and pile up at the inner edge. Thus, there are critical issues of timing and substorm onset definition which require more theoretical and observational attention.

As magnetic reconnection reaches the last closed field lines of the plasma sheet, this would begin to pinch off the tailward plasmoid structure beyond 15-20 R_E. In the present scenario, this would occur at ~ 0111 UT. At this same time we would expect the strongest and most impulsive

energetic particle production (Baker and Belian, 1986), and these particles should rapidly propagate both earthward and tailward. The earthward moving energetic particles would be seen after finite propagation delay as part of an impulsive injection population in the outer trapping region, while the tailward moving particles would, in part at least, fill up the closed plasmoid structure with energetic particles. The large increase of relativistic electrons observed by IMP-8 just a minute or two after the substorm onset (see Fig. 17) and the subsequent episode of southward magnetic field in the plasma sheet would seem to support this picture quite well.

The intense cross-tail current at the inner edge of the plasma sheet late in the growth phase is probably supported by ions in Speiser-type orbits and by anisotropic ($j_{\parallel} > j_{\perp}$) thermal electrons (Mitchell et al., 1990; Baker and McPherron, 1990). As reconnection proceeds to the open field lines of the lobe, the magnetic topology suddenly changes in a very fundamental way. At this point, within the current wedge region, there are no overlying closed flux tubes to restrain the highly distorted and stressed flux tubes in the inner plasma sheet. As soon as the stresses begin to be relieved, the strong pressure gradients represented by the thin, confined current sheet would tend to expand the plasma confinement region as we have inferred in Fig. 13. The more the current sheet expands, the larger becomes the radius of curvature of the field lines passing through the equatorial plane. Thus, the plasma gradients weaken and the curvature drifts diminish so that the cross-tail current weakens rapidly in almost a "positive feedback" sense. Hence, there would be strong diversion of current to the ionosphere from the inner edge of the plasma sheet, but there would also be a reduction of cross-tail current density just due to the relieved field stresses within the current wedge sector.

Careful examination of many auroral images at substorm onset has revealed that auroral brightenings often occur relatively far equatorward of the putative open-closed field line boundary between the polar cap and the low-altitude extention of the plasma sheet (Murphree et al., 1991; 1992). The case under study here clearly shows such behavior (see Fig. 3 and Fig. 15) since we see that the auroral intensification at ~ 0112 UT occurred most prominently at MLAT $\leq 60^{\circ}$, while the auroral oval region extended rather evidently to MLAT > 65°. Thus, the brightening aurora clearly could not map directly to a region of the plasma sheet in which open field lines were reconnecting. Our interpretation (Fig. 18) above was that the initially brightening aurora mapped to a region quite near the Earth (~ 8-12 R_E), while the most intense westward electrojet currents mapped to a region deeper (15-20 R_E) in the tail. We have argued that the abrupt onset of the substorm (~ 0111 UT) corresponded to explosive reconnection of low -ß flux tubes. If, as seems to be the case, detailed mapping shows that there are closed field lines in this case even poleward of the substorm westward electrojet current flow, then we would argue that the substorm onset

corresponds to reconnection of plasma sheet boundary layer (PSBL) field lines, not strictly open lobe field lines. PSBL flux tubes correspond to regions of lower density and higher field strength (i.e., lower β) compared to the central plasma sheet. In this picture, the merging of lobe field lines would occur a minute or two after the substorm onset and only then would the severance of a plasmoid, etc. occur. This would perhaps be consistent with the slightly later observation of southward field and particle enhancements seen at IMP-8 (Fig. 17).

An interesting feature of this event is the fact that B_Z started to increase rather substantially and systematically at all high altitude spacecraft locations (ISEE-1, GOES-5, SCATHA) at almost precisely 0111 UT. Yet, the B_X component did not begin to decrease at any of these locations at that time, but rather the X-component seemed to increase, if anything, for several more minutes. The diminishing B_Z, therefore, seems to be a rather global effect which we might associate with a broad enhancement of the field-aligned currents possibly due to the enhancement of reconnection across a major fraction of the magnetotail (Fig. 18) as PSBL field lines began to merge. On the other hand in the nearer tail, the current wedge per se seemed to start in a localized region (Fig. 12) and the near Earth cross-tail current was not disrupted completely for many minutes after the onset. This disruption proceeded in a sequential way as the full wedge current system was established across a broadening part of the tail. Thus, we see evidence in all of these observations that a broad, global onset occurred at 0111 UT affecting the entire pre-midnight sector (probably associated with the fundamental, driving features of the neutral line) and we also see the localized, sequentially spreading disruption of cross-tail currents in the nearer-Earth region after the initial onset.

SUMMARY

We have studied an intense substorm event on 3 May 1986 occurring toward the end of a strong storm period. The auroral electrojet indices and global imaging data from both the northern and southern hemispheres revealed clearly the growth phase and expansion phase development for a substorm with onset at 0111 UT. For the present study we have had a combination of several new, or seldom before available, tools:

- An ideally located constellation of four spacecraft allowed detailed observation of the substorm growth phase in the near-tail region;

- A realistic time-evolving magnetic field model provided a global representation of the field configuration throughout the growth and early expansion phase of the substorm;

- The substorm initiation was well-observed in both the northern and southern hemisphere by global auroral imagers; and

- Concurrent measurements were made in the mid- to distant-tail region showing both the energy storage (growth) phase and onset (expansion) phase development.

We find evidence of a narrowly localized substorm onset region in the near-Earth tail. This region spread rapidly eastward and poleward after the 0111 UT onset. Our approach in this study was also novel in that:

- Auroral features and their spreading in longitude and latitude were studied in a conjugate sense using the realistic 3-D magnetic field model;

- Auroral structures were mapped to the equatorial plane and the time-evolution was directly compared with multispacecraft particle and field data;

- A clear latitudinal separation ($\geq 10°$) of the initial region of the auroral brightening and the region of most intense westward electrojet current flow was identified;

- We developed further the notion (Pulkkinen et al., 1991) that the region of initial auroral brightening mapped into the near-tail equatorial plane in a region of strong thermal electron chaotization;

- IMP-8 data in the mid-tail region showed signatures of strong energetic particle enhancement, strong plasma flow, and southward magnetic field consistent with a plasmoid or flux rope structure; and

- A comprehensive interpretation of this event was presented in terms of a modification of the standard near-Earth neutral line model (Fig. 18).

We conclude that these results are consistent with a model of late growth phase formation of a magnetic neutral line. This reconnection region caused plasma sheet current diversion before the substorm onset and eventually led to cross-tail current disruption at the time of the substorm onset.

References

Anger, C. D., S. K. Babey, A. L. Broadfoot, R. G. Brown, L. L. Cogger, R. Gattinger, J. W. Haslett, R. A. King, D. J. McEwen, J. S. Murphree, E. H. Richardson, B. R. Sandel, K. Smith, and A. Vallance Jones, An ultraviolet auroral imager for the Viking spacecraft, *Geophys. Res. Lett.*, **14**, 387-390, 1987.

Atkinson, G., An approximate flow equation for geomagnetic flux tubes and its application to polar substorms, *J. Geophys. Res.*, **72**, 5373, 1967.

Axford, W. I., Magnetic field reconnection, in *Magnetic Reconnection in Space and Laboratory Plasmas, Geophys. Monogr. Ser.*, vol. 30, edited by E. W. Hones, Jr., p. 1, AGU, Washington, DC, 1984.

Baker, D. N., and R. D. Belian, Impulsive ion acceleration Earth's outer magnetosphere, in *Ion Acceleration in the Magnetosphere and Ionosphere, Geophys. Monogr. Ser.*, vol. 38, edited by T. Chang, p. 375, AGU, Washington, DC, 1986.

Baker, D. N., and R. L. McPherron, Extreme energetic particle decreases near geostationary orbit: A manifestation of current diversion within the inner plasma sheet, *J. Geophys. Res.*, **95**, 6591, 1990.

Baker, D. N., and T. I. Pulkkinen, The Earthward edge of the plasma sheet in magnetospheric substorms, in *Magnetospheric Substorms, Geophys. Monogr.*, vol. 64, p. 147, AGU, Washington, DC, 1991.

Baker, D. N., and E. C. Stone, Energetic electron anisotropies in the magnetotail: Identification of open and closed field lines, *Geophys. Res. Lett.*, **3**, 557, 1976.

Baker, D. N., and E. C. Stone, Observations of energetic electrons (E > 200 keV) in the earth's magnetotail: Plasma sheet and fireball observations, *J. Geophys. Res.*, **82**, 1532, 1977.

Baker, D. N., P. R. Higbie, E. W. Hones, Jr., and R. D. Belian, High-resolution energetic particle measurements at 6.6 R_E. Low-energy electron anisotropies and short-term substorm predictions, *J. Geophys. Res.*, **83**, 4863, 1978.

Baker, D. N., E. W. Hones, Jr., P. R. Higbie, R. D. Belian, and P. Stauning, Global properties of the magnetosphere during a substorm growth phase: A case study, *J. Geophys. Res.*, **86**, 8941, 1981.

Baker, D. N., S.-I. Akasofu, W. Baumjohann, J. W. Bieber, D. H. Fairfield, E. W. Hones, Jr., B. H. Mauk, R. L. McPherron, and T. E. Moore, "Substorms in the magnetosphere," Chapter 8 of *Solar Terrestrial Physics - Present and Future*, NASA Pub. 1120, Washington, DC, 1984.

Birn, J., and M. Hesse, The substorm current wedge and field-aligned currents in MHD simulations of magnetotail reconnection, *J Geophys. Res*, **96**, 1611, 1991.

Birn, J., E. W. Hones, Jr., J. D. Craven, L. A. Frank, R. D. Elphinstone, J. S. Murphree, and D. P. Stern, On open and closed field line regions in Tyganenko's field model and their possible associations with horse collar auroras, *J. Geophys. Res.*, **96**, 3811, 1991.

Büchner, J., and L. M. Zelenyi, Chaotization of the electron motion as the cause of an internal magnetotail instability and substorm onset, *J. Geophys. Res.*, **92**, 13456, 1987.

Büchner, J. and L. M. Zelenyi, Regular and chaotic charged particle motion in magnetotaillike field reversals 1. Basic theory of trapped motion, *J. Geophys. Res.*, **94**, 11821, 1989.

Craven, J. D., and L. A. Frank, Diagnosis of auroral dynamics using global imaging with emphasis on large-scale evolutions, in *Auroral Physics*, Ed. by C.-I. Meng, M. J. Rycroft, and L. A. Frank, Cambridge Univ. Press, 1991.

Davis, T. N., and M. Sugiura, Auroral electrojet activity index AE and its Universal Time variations, *J. Geophys. Res.*, **71**, 785, 1966.

Elphinstone, R. D. and D. J. Hearn, Mapping of the auroral distribution during quiet times and substorm recovery, *Proceedings from ICS-1 Conference*, Kiruna, in press, 1992.

Elphinstone, R. D., D. Hearn, J. S. Murphree and L. L. Cogger, Mapping using the Tsyganenko long magnetospheric model and its relationship to Viking auroral images, *J. Geophys. Res.*, **96**, 1467, 1991.

Fairfield, D. H., R. P. Lepping, E. W. Hones, Jr., S. J. Bame, and J. R. Asbridge, Simultaneous measurements of magnetotail dynamics of IMP spacecraft, *J. Geophys. Res.*, **86**, 1396, 1981.

Fennell, J. F., Description of P78-2 (SCATHA) satellite and experiments, in *The IMS Source Book* (eds. C. T. Russell and D. J. Southwood), p. 65, AGU, Washington, DC, 1982.

Frank, L. A., K. L. Ackerson, and R. P. Lepping, On hot tenuous plasmas, fireballs, and boundary layers in the earth's magnetotail, *J. Geophys. Res.*, **81**, 5859, 1976.

Frank, L. A., D. M. Yeager, H. D. Owens, K. L. Ackerson, and M. R. English, Quadrispherical LEPEDEAS for ISEE-1 and -2 plasma measurements, *IEEE TRANS. GEOSC ELEC.*, **GE-16**, 221, 1978.

Frank, L A., J. D. Craven, K. L. Ackerson, M. R. English, R. H. Eather, and R. L. Carovillano, Global auroral imaging instrumentation for the Dynamics Explorer Mission, *Space Sci. Instrum.*, **5**, 369, 1981.

Hesse, M. and J. Birn, On dipolarization and its relation to the substorm current wedge, *J. Geophys. Res.*, **96**, 19417, 1991.

Hones, E. W., Jr., Substorm processes in the magnetotail: Comments on "On hot tenuous plasmas, fireballs, and boundary layers in the earth's magnetotail" by L. A. Frank, K. L. Ackerson, and R. P. Lepping, *J. Geophys. Res.*, **82**, 5633, 1977.

Hones, E. W., Jr., Project PROMIS to coordinate satellites, *EOS*, **66**, 1369, 1985.

Hones, E. W., Jr., C. D. Anger, J. Birn, J. S. Murphree, and L. L. Cogger, A study of a magnetospheric substorm recorded by the VIKING auroral imager, *Geophys. Res. Lett.*, **14**, 411, 1987.

Hughes, W. J., and D. G. Sibeck, On the 3-dimensional structure of plasmoids, *Geophys. Res. Lett.*, **14**, 636, 1987.

Kaufmann, R. L. Substorm currents: Growth phase and onset, *J. Geophys. Res.*, **92**, 7471, 1987.

Lui, A. T. Y., D. J. Williams, T. E. Eastman, L. A. Frank, and S. I. Akasofu, Streaming reversal of energetic particles in the magnetotail during a substorm, *J. Geophys. Res.*, **89**, 1540, 1984.

Lui, A. T. Y., Estimates of current changes in the geomagnetic tail associated with a substorm, *Geophys. Res. Lett.*, **5**, 853, 1978.

McPherron, R. L., Growth phase of magnetospheric substorms, *J. Geophys. Res.*, **75**, 5592, 1970.

McPherron, R. L., C. T. Russell, and M. A. Aubry, Satellite studies of magnetospheric substorms on August 15, 1968, A phenomenological model for substorms, *J. Geophys. Res.*, **78**, 3131, 1973.

Mitchell, D. G., D. J. Williams, C. Y. Huang, L. A. Frank, and C. T. Russell, Current carriers in the near-Earth cross-tail current sheet during substorm growth phase, *Geophys. Res. Lett.*, **17**, 583, 1990.

Murphree, J. S., R. D. Elphinstone, D. Hearn, and L. L. Cogger, Interpretation of optical substorm onset observations, *J. Atmos. Terr. Phys.*, in press, 1992.

Murphree, J. S., R. D. Elphinstone, L. L. Cogger, and D. Hearn, Viking optical substorm signatures, *in Magnetospheric Substorms, AGU Monograph, Vol. 64,* edited by J. R. Kan, T. A. Potemra, S. Kokubun, and T. Ijima, pg. 241, 1991.

Nagai, T., Observed magnetic substorm signatures at synchronous altitude, *J. Geophys. Res.*, **87**, 4405, 1982.

Nagai, T., D. N. Baker, and P. R. Higbie, Development of substorm activity in multiple-onset substorms at synchronous orbit, *J. Geophys. Res.*, **88**, 6994, 1983.

Pulkkinen, T. L., A study of magnetic field and current configurations in the magnetotail at time of a substorm onset, *Planet. Space Sci.*, **39**, 883, 1991.

Pulkkinen, T. I., D. N. Baker, D. H. Fairfield, R. J. Pellinen, J. S. Murphree, R. D. Elphinstone, R. L. McPherron, J. F. Fennell, R. E. Lopez, and T. Nagai, Modeling the growth phase of a substorm using the Tsyganenko model and multi-spacecraft observations: CDAW-9, *Geophys. Res. Lett.*, **18**, 1963, 1991.

Pulkkinen, T. I., D. N. Baker, R. J. Pellinen, J. Büchner, H. E. J. Koskinen, R. E. Lopez, R. L. Dyson, and L. A. Frank, Particle scattering and current sheet stability in the geomagnetic tail during the substorm growth phase, *J. Geophys. Res.*, in press, 1992.

Rostoker, G., S.-I. Akasofu, J. Foster, R. A. Greenwald, Y. Kamide, K. Kawasaki, A. T. Y. Lui, R. L. McPherron, and C. T. Russell, Magnetospheric substorms - definition and signatures, *J. Geophys. Res.*, **85**, 1663, 1980.

Russell, C. T., The ISEE-1 and -2 fluxgate magnetometers, *IEEE Trans. Geosc. Electr.*, **GE-16**, 239, 1978.

Sarris, E. T., D. J. Williams, and S. M. Krimigis, Observations of counterstreaming between plasma and energetic particles in the magnetotail, *J. Geophys. Res.*, **83**, 5655, 1978.

Schindler, K., D. N. Baker, J. Birn, E. W. Hones, Jr., J. A. Slavin, and A. B. Galvin, A study of strong earthward plasma flow at ~200 R_E in Earth's magnetotail: CDAW-8, *J. Geophys. Res.*, **94**, 15177, 1989.

Scholer, M., G. Gloeckler, B. Klecker, F. M. Ipavich, D. Hovestadt, and E. J. Smith, Fast moving plasma structures in the distant magnetotail, *J. Geophys. Res.*, **89**, 6717, 1984.

Scholer, M., D. N. Baker, S. J. Bame, W. Baumjohann, G. Gloeckler, E. J. Smith, and B. T. Tsurutani, Correlated observations of substorm effects in the near Earth region and the distant magnetotail, *J. Geophys. Res.*, **90**, 4021, 1985.

Sergeev, V. A., P. Tanskanen, K. Mursala, A. Korth, and R. C. Elphic, Current sheet thickness in the new earth plasma sheet during substorm growth phase, *J. Geophys. Res.*, **95**, 3819, 1990.

Tsyganenko, N. A., Global quantitative models of the geomagnetic field in the cislunar magnetosphere for different disturbance levels, *Planet. Space Sci.*, **35**, 1347, 1987.

Tsyganenko, N. A., Magnetospheric magnetic field model with a warped tail current sheet, *Planet. Space Sci.*, **37**, 5, 1989.

Vasyliunas, V. M., Theoretical models of magnetic field line merging, *Rev. Geophys.*, **13**, 303, 1975.

TECHNOLOGY OPERATIONS

The Aerospace Corporation functions as an "architect-engineer" for national security programs, specializing in advanced military space systems. The Corporation's Technology Operations supports the effective and timely development and operation of national security systems through scientific research and the application of advanced technology. Vital to the success of the Corporation is the technical staff's wide-ranging expertise and its ability to stay abreast of new technological developments and program support issues associated with rapidly evolving space systems. Contributing capabilities are provided by these individual Technology Centers:

Electronics Technology Center: Microelectronics, solid-state device physics, VLSI reliability, compound semiconductors, radiation hardening, data storage technologies, infrared detector devices and testing; electro-optics, quantum electronics, solid-state lasers, optical propagation and communications; cw and pulsed chemical laser development, optical resonators, beam control, atmospheric propagation, and laser effects and countermeasures; atomic frequency standards, applied laser spectroscopy, laser chemistry, laser optoelectronics, phase conjugation and coherent imaging, solar cell physics, battery electrochemistry, battery testing and evaluation.

Mechanics and Materials Technology Center: Evaluation and characterization of new materials: metals, alloys, ceramics, polymers and their composites, and new forms of carbon; development and analysis of thin films and deposition techniques; nondestructive evaluation, component failure analysis and reliability; fracture mechanics and stress corrosion; development and evaluation of hardened components; analysis and evaluation of materials at cryogenic and elevated temperatures; launch vehicle and reentry fluid mechanics, heat transfer and flight dynamics; chemical and electric propulsion; spacecraft structural mechanics, spacecraft survivability and vulnerability assessment; contamination, thermal and structural control; high temperature thermomechanics, gas kinetics and radiation; lubrication and surface phenomena.

Space and Environment Technology Center: Magnetospheric, auroral and cosmic ray physics, wave-particle interactions, magnetospheric plasma waves; atmospheric and ionospheric physics, density and composition of the upper atmosphere, remote sensing using atmospheric radiation; solar physics, infrared astronomy, infrared signature analysis; effects of solar activity, magnetic storms and nuclear explosions on the earth's atmosphere, ionosphere and magnetosphere; effects of electromagnetic and particulate radiations on space systems; space instrumentation; propellant chemistry, chemical dynamics, environmental chemistry, trace detection; atmospheric chemical reactions, atmospheric optics, light scattering, state-specific chemical reactions and radiative signatures of missile plumes, and sensor out-of-field-of-view rejection.

THE AEROSPACE CORPORATION
2350 E. El Segundo Boulevard
El Segundo, California 90245-4691
U.S.A.